Autophagy

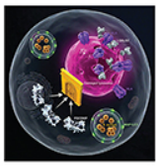

Autophagy

ISSN: 1554-8627 (Print) 1554-8635 (Online) Journal homepage: www.tandfonline.com/journals/kaup20

CHCHD2 and CHCHD10 promoted autophagic clearance of protein aggregates via GABARAPs

Wei Zhou, Maggie Menglan Zhang , Willcyn Tang, Brijesh Kumar Singh, Zhiwei Zhang , Lei Zhou , Jaron Kim Wee Goh , Faith Rui En Tan , Jingxiu Huang , Qiaoyang Sun, Bin Xiao , Gupta Priyanka , Alfred Xuyang Sun, Li Zeng, Han-Ming Shen & Eng King Tan

To cite this article: Wei Zhou, Maggie Menglan Zhang , Willcyn Tang, Brijesh Kumar Singh, Zhiwei Zhang , Lei Zhou , Jaron Kim Wee Goh , Faith Rui En Tan , Jingxiu Huang , Qiaoyang Sun, Bin Xiao , Gupta Priyanka , Alfred Xuyang Sun, Li Zeng, Han-Ming Shen & Eng King Tan (01 Jul 2026): CHCHD2 and CHCHD10 promoted autophagic clearance of protein aggregates via GABARAPs, Autophagy, DOI: 10.1080/15548627.2026.2678427

To link to this article: https://doi.org/10.1080/15548627.2026.2678427

AUTOPHAGY
https://doi.org/10.1080/15548627.2026.2678427

Taylor & Francis
by informa

RESEARCH PAPER

OPEN ACCESS Check for updates

CHCHD2 and CHCHD10 promoted autophagic clearance of protein aggregates via GABARAPs

Wei Zhou [a], Maggie Menglan Zhang[b], Willcyn Tang [b], Brijesh Kumar Singh [c], Zhiwei Zhang[d], Lei Zhou[e,f], Jaron Kim Wee Goh[g], Faith Rui En Tan[g], Jingxiu Huang[b,h], Qiaoyang Sun [a], Bin Xiao[a], Gupta Priyanka[c], Alfred Xuyang Sun [a,b], Li Zeng [d], Han-Ming Shen [i], and Eng King Tan [a,b,j]

[a]Department of Research, National Neuroscience Institute, Singapore, Singapore; [b]Signature Research Program in Neuroscience and Behavioural Disorders, Duke-NUS Graduate Medical School, Singapore, Singapore; [c]Signature Research Program in Cardiovascular and Metabolism Disorders, DUKE-NUS Graduate Medical School, Singapore, Singapore; [d]Neural Stem Cell Research Laboratory, Department of Research, National Neuroscience Institute, Singapore, Singapore; [e]School of Optometry, Department of Applied Biology and Chemical Technology, Research Centre for SHARP Vision (RCSV), Hong Kong Polytechnic University, Hong Kong, China; [f]Centre for Eye and Vision Research (CEVR), Hong Kong, China; [g]School of Life Sciences and Chemical Technology, Ngee Ann Polytechnic, Singapore, Singapore; [h]Department of Anaesthesiology, State Key Laboratory of Oncology in South China, Sun Yat-sen University Cancer Cener, Guangzhou, China; [i]Faculty of Health Sciences, Ministry of Education Frontiers Science Centre for Precision Oncology, University of Macau, Macau, China; [j]Department of Neurology, National Neuroscience Institute, Singapore, Singapore

ABSTRACT

Mutations in mitochondrial protein CHCHD2 and its paralog CHCHD10 were identified in patients with Parkinson disease (PD), amyotrophic lateral sclerosis (ALS), frontotemporal dementia (FTD) or Alzheimer disease (AD). CHCHD2 and CHCHD10 mutations caused neurodegeneration in model animals as seen in patients, but their pathophysiological roles remain elusive. Here we reported a direct role of CHCHD2 and CHCHD10 in autophagy. We identified a protein complex composing of CHCHD2-CHCHD10-C1QBP/p32-Atg8-family proteins (ATG8s), in which each molecule interacted with another. CHCHD2, CHCHD10 and C1QBP/p32 associated with ATG8s, preferentially, GABARAPs. Disease-associated CHCHD2 and CHCHD10 mutations exhibited varied interaction with ATG8s. By binding to GABARAPs, CHCHD2 and CHCHD10 underwent autophagic degradation, and recruited the ULK1 complex. Autophagy initiation defects occurred upon transient knockdown of *CHCHD2*, and also in human iPSC-derived *CHCHD2*$^{-/-}$ or *CHCHD2*^{T61I} dopaminergic neurons. Importantly, CHCHD2 and CHCHD10 promoted autophagy. CHCHD2 reduced protein aggregates in cells and toxic SNCA/α-synuclein species in mouse striatum. Our study thus revealed mitochondrial proteins CHCHD2 and CHCHD10 as both autophagy substrates and autophagy activators and laid groundwork for therapy targeting patients with neurodegeneration.

ARTICLE HISTORY
Received 14 September 2025
Revised 12 May 2026
Accepted 19 May 2026

KEYWORDS
Aggregates; autophagy; CHCHD10; CHCHD2; GABARAPs; neurodegeneration

Abbreviations: AA: amino acid; AD: Alzheimer disease; ALS: amyotrophic lateral sclerosis; ATG5: autophagy related 5; ATG7: autophagy related 7; ATG8: mammalian Atg8-family protein; ATG13: autophagy related 13; bafA1: bafilomycin A_1; C1QBP/p32/gC1qR/HABP1: complement component 1, q subcomponent binding protein; CHCHD2/MNRR1/MIX17B: coiled-coil-helix-coiled-coil-helix domain containing 2; CHCHD10/MIX17A: coiled-coil-helix-coiled-coil-helix domain containing 10; CHX: cycloheximide; CMA: chaperone-mediated autophagy; CRISPR: clustered regularly interspaced short palindromic repeats; CQ, chloroquine; DA: dopaminergic; DMSO: dimethyl sulfoxide; EBSS: Earle's balanced salt solution; RB1CC1/FIP200: RB1 inducible coiled-coil 1; FTD: frontotemporal dementia; GABARAP: gamma-aminobutyric acid receptorbassociated protein; GABARAPL1: GABA type A receptor associated protein like 1; GABARAPL2: GABA type A receptor associated protein like 2; hESC: human embryonic stem cells; iPSC: induced pluripotent stem cell; KO: knockout; LAMP1: lysosomal-associated membrane protein 1; LAMP2A: lysosomal-associated membrane protein 2A; MAP1LC3/LC3: microtubule-associated protein 1 light chain 3; LIR: LC3-interacting region; PD: Parkinson disease; SQSTM1/p62: sequestosome 1; TARDBP/TDP-43: TAR DNA binding protein; TH: tyrosine hydroxylase; TMR, tetramethylrhodamine; WT: wild type; UB: ubiquitin; ULK1: unc-51 like kinase 1.

Introduction

Neurodegenerative disorders including Parkinson disease (PD), amyotrophic lateral sclerosis (ALS), frontotemporal dementia (FTD) and Alzheimer disease (AD) are characterized with neuron loss with mitochondrial dysfunction and protein aggregates. Disruption of either mitochondria or proteostasis leads to

CONTACT Wei Zhou zhou.wei@sgh.com.sg; Tan Eng King tan.eng.king@singhealth.com.sg Department of Research, National Neuroscience Institute, The Academia, 20 College Road, Singapore 169856, Singapore

Supplemental data for this article can be accessed online at https://doi.org/10.1080/15548627.2026.2678427.

neurodegeneration; however, those pathogenic mechanisms are always heavily entangled, providing challenges in designing efficient interventions.

Mitochondrial protein CHCHD2/MNRR1/MIX17B (coiled-coil-helix-coiled-coil-helix domain containing 2) and its paralog CHCHD10/MIX17A (coiled-coil-helix-coiled-coil-helix domain containing 10) are associated with various neurodegenerative disorders. Heterozygous *CHCHD2*^{T61I} mutant was firstly identified in a late-onset autosomal dominant PD family with Lewy bodies [1], and later in patients with PD [2–6], AD [7,8], essential tremor [9], FTD [7,8] or ALS [8,10,11]. CHCHD2 binds to its paralog CHCHD10 [12–14], sharing 57% sequence identity. CHCHD10 mutations were identified in neurodegenerative or motor neuron disorders including FTD [15–18], ALS [15,16,19], mitochondrial myopathy [20], CMT2 (Charcot-Marie-Tooth disease type 2) [21], SMAJ (spinal muscular atrophy, Jokela type) [22] and PD [6]. CHCHD2 or CHCHD10 mutations caused neurodegeneration with protein aggregates in C. elegans [23], Drosophila melanogaster [24–27], zebrafish [28] and mouse [29–38], similarly seen in patients [39,40]. However, their underlying physiological roles remain elusive.

As mitochondrial proteins, CHCHD2 and CHCHD10 locate in the mitochondrial intermembrane space [41] and associate with mitochondrial inner membrane [14]. They maintain mitochondrial inner membrane ultrastructure, regulate mitochondrial stress response, metabolism and apoptosis [12,14,24,42,43]. Such roles appear to explain neurodegeneration caused by CHCHD2 or CHCHD10 mutants, but *chchd2 and chchd10* double knockout (DKO) mice or *CHCHD2 and CHCHD10* DKO iPSCs (induced pluripotent stem cells) were largely normal with some mitochondria defects [44,45], suggesting mitochondrial roles of CHCHD2 and CHCHD10 are largely dispensable and neurodegeneration caused by mutations in CHCHD2 or CHCHD10 may not be due to their mitochondrial functions. Moreover, how do CHCHD2 or CHCHD10 mutations cause aggregates? Some CHCHD2 or CHCHD10 mutants formed aggregates [31,35,36,46]. CHCHD2 colocalized with Lewy bodies in PD patient [47], but CHCHD2 did not bind to SNCA/α-synuclein [29]. CHCHD10 instead bound to TARDBP/TDP-43 (TAR DNA binding protein 43) [23]. CHCHD10 aggregates colocalized with TARDBP inclusions in FTD or AD patients [34], but this cannot explain how CHCHD10 mutants associated with protein aggregates absent of TARDBP pathology [48]. Notably, *chchd2*$^{-/-}$ mice showed autophagy defects [29]. CHCHD10 aggregates were found in midbrain neurons in juvenile *Chchd10*^{S59L} mice, a stage before mitochondria dysfunction occurred [34,35,49], suggesting CHCHD2 and CHCHD10 play roles in proteostasis, possibly preceding their mitochondrial functions.

CHCHD2 and CHCHD10 associate with C1QBP/p32/gC1qR/HABP1 (complement component 1, q subcomponent binding protein) [41,50,51], an abundant mitochondrial matrix protein. C1QBP/p32 is indispensable for mitochondria by exerting numerous functions [52]. Biallelic or homozygous C1QBP/p32 mutations were reported in human patients with severe or fatal clinical manifestations [53–56]. Central nervous system-specific *c1qbp*$^{-/-}$ mice died within 8 weeks of birth showing degenerative phenotypes [57]. Cardiomyocyte-specific *c1qbp*$^{-/-}$ mice were embryonic lethal with autophagic abnormalities [58,59]. The central role of C1QBP/p32 underlying such severity seems vague with its pleiotropic cellular functions.

Here we investigated CHCHD2 and CHCHD10's roles in macroautophagy/autophagy-lysosome pathway. We discovered a protein complex composing of CHCHD2-CHCHD10-C1QBP/p32-ATG8s (autophagy related 8), in which every molecule bound to another. CHCHD2, CHCHD10 and C1QBP/p32 preferentially bound to GABARAPs (GABA type A receptor-associated protein), so that CHCHD2 and CHCHD10 functioned as both autophagy substrates and activators. Our study thus revealed direct roles of CHCHD2-CHCHD10-C1QBP/p32 complex in autophagy and provided novel perspectives on mitochondria in global protein homeostasis.

Results

CHCHD2 and CHCHD10 underwent active autophagic degradation via lysosomes

CHCHD2, CHCHD10 and C1QBP are mitochondrial proteins, binding to each other. Consistent with previous studies [13,41], CHCHD2 degraded fast, with a t1/2 ≤ 2 h. CHCHD10 had a slightly longer t1/2 than CHCHD2, while C1QBP was stable (Figure 1(A)). To examine how CHCHD2 decayed, we tested if CHCHD2 was decayed by mitochondrial proteases. CHCHD2 or CHCHD10 was reduced upon knockdown of mitochondrial proteases LONP1 (lon peptidase 1, mitochondrial), CLPP (caseinolytic mitochondrial matrix peptidase proteolytic subunit), HTRA2 (HtrA serine peptidase 2), YME1L1 (YME1-like 1 (S. cerevisiae)), AFG3L2 (AFG3-like AAA ATPase 2) (Figures S1A-B), or LONP1 inhibitor treatment (Figures S1C), suggesting those mitochondrial proteases could play more roles in stabilizing CHCHD2 and CHCHD10 than degrading them. Mitochondrial uncoupler FCCP, inducing PINK1 (PTEN induced putative kinase 1)-PRKN/Parkin (parkin RBR E3 ubiquitin protein ligase)-dependent mitophagy, enhanced CHCHD2 and CHCHD10 [13,60], suggesting neither CHCHD2 nor CHCHD10 was degraded by PINK1-PRKN /Parkin-dependent mitophagy. Next, we tested if CHCHD2 or CHCHD10 was decayed via proteasome. CHCHD2 and CHCHD10 were reduced upon treatment of proteasome inhibitor MG132 or BTZ (bortezomib) (Figure 1(B)), suggesting neither CHCHD2 nor CHCHD10 was degraded by UB (ubiquitin)-dependent proteasome pathway. MAP1LC3/LC3 (microtubule associated protein 1 light chain 3)-II was enhanced by MG132 (Figure 1(B)), indicative of autophagy activation [61]. We then tested if CHCHD2 or CHCHD10 was degraded via autophagy. CHCHD2 was reduced by activation of autophagy via torin1, rapamycin, nutrient deprivation by EBSS (Earle's balanced salt solution) or serum starvation (Figure 1(C), S1D). CHCHD2 and CHCHD10 were enhanced by wortmannin (Wort, an autophagy inhibitor), chloroquine (CQ, an inhibitor of autophagy-lysosome), bafilomycin A_1 (bafA1, inhibitor of vacuolar-type H^+-ATPase) (Figures 1(D-E), S1E-F) and the combination of leupeptin with NH_4Cl which

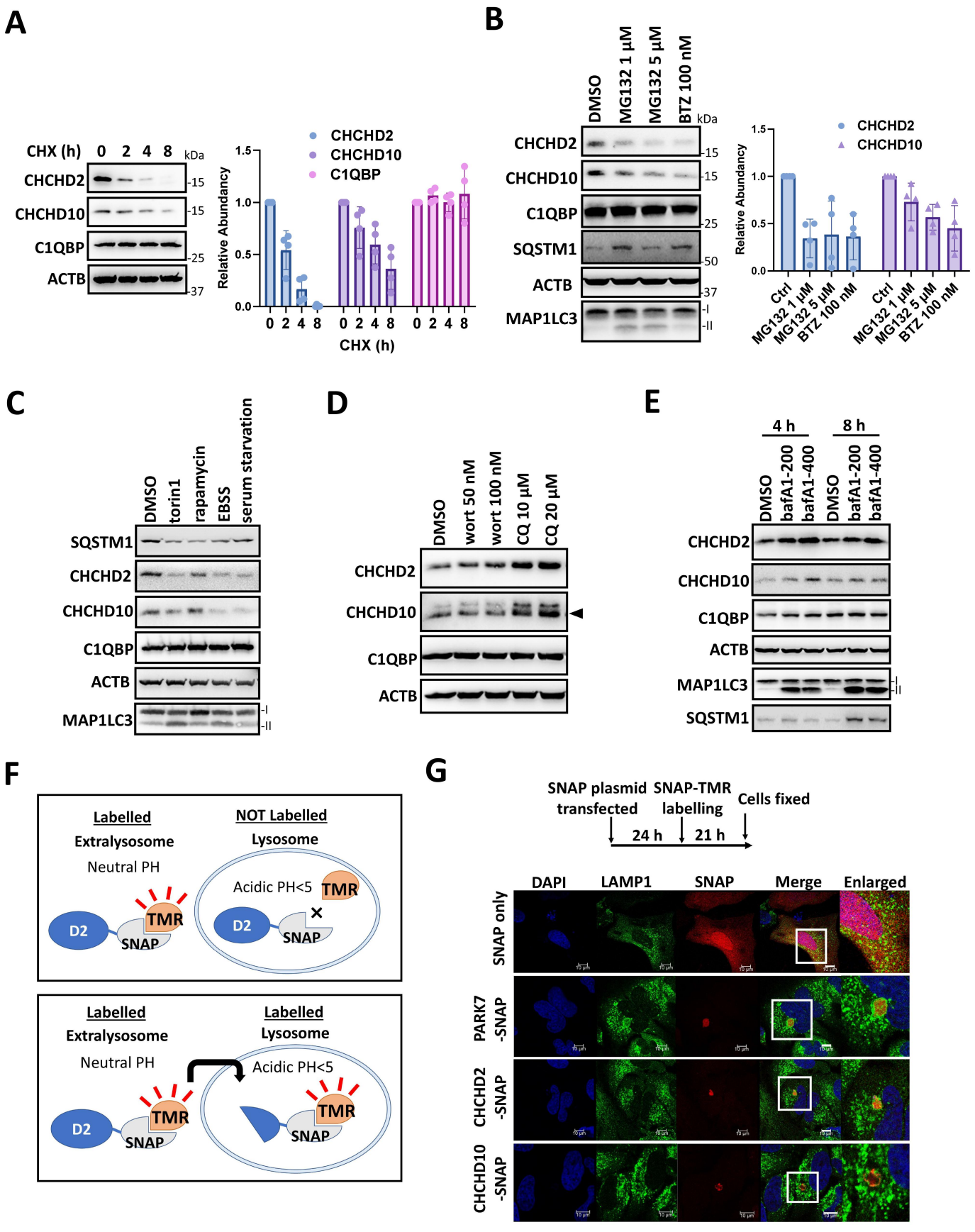

Figure 1. CHCHD2 and CHCHD10 underwent autophagic degradation via lysosomes. (A) Western blot analysis of endogenous CHCHD2, CHCHD10 and C1QBP in SK-N-SH cells treated with protein synthesis inhibitor CHX (cycloheximide) 50 µg/ml. Quantification of CHCHD2, CHCHD10 and C1QBP normalized with ACTB. $n = 4$. (B) Western blot analysis of SK-N-SH cells treated with proteasome inhibitor MG132 1 µM or 5 µM, proteasome inhibitor bortezomib (BTZ) 100 nM for 5 h. Quantification of CHCHD2 and CHCHD10 normalized with ACTB. $n = 4$. (C) Western blot analysis of SK-N-SH cells treated with 250 nM MTOR inhibitor torin1, 10 µM rapamycin,

inhibits lysosomal proteases (Figure S4D). Collectively, CHCHD2 and CHCHD10 were actively degraded via autophagy-lysosome pathway.

We wondered if CHCHD2 and CHCHD10 colocalized with lysosomes. Endogenous CHCHD2, CHCHD10 and C1QBP were in mitochondria with little colocalization with lysosome marker LAMP1 (lysosomal-associated membrane protein 1) (Figure S1G) [14]. Some colocalization of CHCHD2, CHCHD10 or C1QBP with LAMP1 was observed after lysosome inhibitor treatment (Figure S1G), with most CHCHD2, CHCHD10 or C1QBP still in mitochondria. Cytosolic CHCHD2 or CHCHD10 is hardly captured by regular assays, but CHCHD2 and CHCHD10 are believed to be translated in cytosol and transported to mitochondria [62,63]. Some CHCHD2 or CHCHD10 mutants were cytosolic. PD-associated CHCHD2^{Q126X}, losing an intact C-terminal CHCH domain, was in cytosol [14] (Figures S2A-D, F). ALS-associated CHCHD10^{Q108P}, with a mutated Q108 in CHCH domain, was cytosolic [62] (Figures S2E-F). CHCHD2^{Q120P}, an equivalent of CHCHD10^{Q108P} (Figure S2F), was ~100% cytosolic (Figures S2G-J). Collectively, C-terminal CHCH domain of CHCHD2 and CHCHD10 contributed to their mitochondrial targeting. CHCHD10 was transported to mitochondria via CHCHD4/Mia40/TIMM40 (coiled-coil-helix-coiled-coil-helix domain containing 4) [62]. However, CHCHD4 did not affect mitochondrial localization of wild-type (WT) CHCHD2 or CHCHD2^{Q120P} (Figure S2K). CHCHD2^{Q120P} was in the cytosol when co-overexpressed with CHCHD4. Some CHCHD4 colocalized with CHCHD2^{Q120P} in the cytosol, suggesting CHCHD4 may not direct mitochondrial localization of CHCHD2.

The N termini of CHCHD2 and CHCHD10 could contribute to mitochondrial localization with predicted mitochondrial-transportation signal (MTS) (Figure S2L) [32]. To investigated the N or C terminus of CHCHD2 and CHCHD10 in their mitochondrial targeting, we examined the subcellular localization of CHCHD2 and CHCHD10 with or without N- or C-terminal tags (non-tagged, small tag ~1 kDa and large tag ~20 kDa) (Figures S2L, O). With an expression level similar to endogenous proteins (Data not shown), non-tagged CHCHD2 was predominantly localized to mitochondria with minor cytosolic presence (Figures S2M-N). C-terminal FLAG-MYC-tagged CHCHD2 was predominantly located in mitochondria, with about 20–30% present in the cytosol. N-terminal HA-FLAG-tagged CHCHD2 was partially cytosolic (about 30–40%) (Figures S2M-N). Such results suggested CHCHD2 was present in both the cytosol and mitochondria while a small tag at N or C terminus trapped some CHCHD2 in the cytosol. Alternatively, about 70% of non-tagged CHCHD10 was located in mitochondria. C-terminal FLAG-MYC-tagged CHCHD10 or N-terminal HA-FLAG-tagged CHCHD10 showed similar distribution as non-tagged CHCHD10 (Figures S2P-Q), suggesting CHCHD10 was more cytosolic than CHCHD2 and small tags at N or C terminus of CHCHD10 did not affect its cellular distribution. To further test if N- or C-terminal tags affected CHCHD2 or CHCHD10 localization, we constructed CHCHD2 and CHCHD10 plasmids with a large SNAP-tag, 19.4 kDa (Figures S2L, O) at either N or C terminus. SNAP-fused proteins expressed in cells can be labeled by brief extracellular application of a fluorescently labeled SNAP ligand. A positive control of SNAP system, SNAP-COX8A (cytochrome *c* oxidase subunit 8A), an integral protein of the mitochondrial inner membrane, was in mitochondria [64] (Figure S3A), while SNAP alone was in cytosol (Figure S3B). Labeled with fluorescent SNAP ligand, both SNAP-CHCHD2 and CHCHD2-SNAP were mostly in the cytosol with little in mitochondria (Figures S3C-D). Similar results were observed in SNAP-CHCHD10 and CHCHD10-SNAP (Figures S3E-F), suggesting large tags such as SNAP-tag, at the N or C terminus of CHCHD2 or CHCHD10, abolished mitochondrial targeting. C-terminal SNAP-tagged PARK7/DJ-1 (Parkinson disease (autosomal recessive, early onset) 7), a mitochondrial protein involved in PD [65], was also in the cytosol (Figures S3G). Taken together, both N and C termini of CHCHD2 and CHCHD10 contributed to their mitochondrial localization. We then examined if CHCHD2 and CHCHD10 underwent degradation via autophagy-lysosome pathway, which occurs in the cytosol. To visualize if CHCHD2 or CHCHD10 accumulated in lysosomes, we used SNAP-tag system. SNAP-tag covalently binds to a red fluorescent tetramethylrhodamine (TMR) SNAP ligand in cell organelles with neutral pH (cytosol and nucleus) but does not do so in the acidic lysosomes, suggesting only extralysosomal proteins are labeled by a fluorescent SNAP ligand. However, after SNAP-fused proteins are fluorescently labeled in the cytosol and translocated to lysosomes with further cell culture, TMR continues to fluoresce in acid lysosomes (Figure 1(F)) [66]. As a positive control of autophagy-lysosome degradation, we monitored the translocation of PARK7/DJ-1, an autophagy substrate [65], from cytosol to LAMP1-positive lysosomes, while SNAP showed little colocalization with LAMP1 (Figure 1(G)). Using this labeling method, CHCHD2-SNAP and CHCHD10-SNAP were translocated from the cytosol (Figures S3C, E) to concentrated irregular puncta colocalizing with lysosome marker LAMP1 (Figure 1(G)) or LAMP2A (lysosomal-associated membrane protein 2A) (Figure S3H). CHCHD2-SNAP and CHCHD10-SNAP underwent degradation (Figure S3I). These results suggested CHCHD2-SNAP and CHCHD10-SNAP can be transported to lysosomes for degradation. We further tested if there was lysosomal accumulation of CHCHD10^{Q108P}-SNAP, as CHCHD10^{Q108P} was cytosolic (Figure S2E). CHCHD10^{Q108P}-SNAP was translocated from the cytosol to puncta, colocalizing with LAMP1 (Figure S3J), similar as WT CHCHD10-SNAP (Figure 1(G)). To experimentally test the presence of cytosolic CHCHD2 and CHCHD10, we employed subcellular fractionation to obtain cytosolic and mitochondrial fractions.

nutrient deprivation by EBSS for 5 h or serum starvation for 24 h. (D) Western blot analysis of HeLa cells treated with autophagy inhibitors wortmannin (wort) and lysosome inhibitor chloroquine (CQ) for 3 h. (E) Western blot analysis of SK-N-SH cells treated with lysosome inhibitors bafA1 at 200 or 400 ng/ml. (F) The labelling strategy of CHCHD2-SNAP or CHCHD10-SNAP by SNAP-Cell® TMR-Star. D2, CHCHD2. (G) Confocal imaging of CHCHD2 or CHCHD10, labelled with SNAP-Cell® TMR-Star (red) and endogenous LAMP1 (green), using the labelling strategy showed in F. SNAP only, negative control. PARK7-SNAP, positive control. Scale bar: 10 μm.

Proteins in cytosolic fraction were concentrated by TCA (trichloroacetic acid) precipitation and redissolved. Mitochondrial markers including TOMM20 (mitochondrial outer membrane protein), TIMM50 (mitochondrial inner membrane protein), COX4I1 (mitochondrial inner membrane protein), and PDH (pyruvate dehydrogenase; mitochondrial matrix protein) showed enrichment in mitochondrial fraction but not cytosolic fraction. As current mitochondria extraction methods usually extract mitochondria accompanied with ER, Golgi and other membrane structures associated to mitochondria, cytosol marker ACTB is always seen in mitochondrial fraction. With such fractionation, CHCHD2 and CHCHD10 were present in the cytosol and mitochondria (Figures S3K-L). C1QBP showed similarly, enriched in mitochondria but also was present in cytosol.

With CHCHD2-SNAP colocalizing with LAMP2A (Figure S3H), the key mediator of CMA, we asked if CHCHD2 was a substrate of chaperone-mediated autophagy (CMA). CMA substrates bound to chaperone HSPA8/HSC70 (heat shock protein family A (Hsp70) member 8) and were then sent to lysosomes for degradation [67]. We identified 2 putative HSPA8 binding motifs KFERQ in CHCHD2, near disease-related CHCHD2^{Q126X} and CHCHD2^{R145Q} (Figures S4A). WT CHCHD2 and CHCHD2^{T61I} bound to HSPA8 (Figure S4B). CHCHD2^{Q126X}, which lost its C terminus including the 2nd putative HSPA8 binding motif KEFRQ, showed reduced binding to HSPA8. CHCHD2^{R145Q}, showed a reduced binding to HSPA8 (Figure S4B). Transient knockdown of *LAMP2A* with 3 isoform-specific siRNAs did not enhance CHCHD2 or CHCHD10 (Figure S4C). LAMP2A overexpression did not reduce CHCHD2 (Figure S4D). CMA-specific inhibitor AR-7 [68] seemed not to affect CHCHD2 or CHCHD10 (Figure S4E). Thus, it is unlikely that CHCHD2 was a substrate of CMA even CHCHD2 bound to HSPA8.

CHCHD2, CHCHD10 and C1QBP independently associated with ATG8s

CHCHD2 binds to CHCHD2, CHCHD10 and C1QBP, while CHCHD10 forms homodimer and C1QBP forms trimer [69], indicating CHCHD2 and CHCHD10 are parts of a large protein complex. In order to search for novel interactors of CHCHD2 and CHCHD10 which explain their roles in autophagy-lysosome pathway, we prepared bacterial purified GST-CHCHD2 and GST-CHCHD10 proteins with purity > 95% (Figure S5A). GST-CHCHD2 and GST-CHCHD10 pulled down endogenous CHCHD2, CHCHD10 and C1QBP (Figure S5B), suggesting purified GST-CHCHD2 and GST-CHCHD10 protein folded properly so that they interacted with their known partners. We used GST-CHCHD2 and GST-CHCHD10 as baits to search for novel binding partners by mass spectrometry. One peptide from GABARAP was captured using GST-CHCHD10 as bait (Figure 2(A)). GABARAP is a member of ATG8 family, including MAP1LC3A/LC3A, MAP1LC3B/LC3B, MAP1LC3C/LC3C, GABARAP, GABARAPL1 (GABA type A receptor-associated protein like 1) and GABARAPL2 (GABA type A receptor associated- protein like 2) [70]. To confirm a direct ATG8-CHCHD10 interaction, we carried out in vitro protein-protein interaction assays with purified recombinant proteins of GST- or His-tagged CHCHD10, CHCHD2 and C1QBP, along with His- or GST-tagged ATG8s (Figure 2(B-D), S5C-D). His-CHCHD10 bound to ATG8s, with a preference for GABARAPL1 and GABARAPL2 (Figure 2(B)). Meanwhile, a weak interaction between His-CHCHD2 and GST-GABARAPL1 or GST-GABARAPL2 was seen (Figure 2(C)). Unexpectedly, His-C1QBP protein bound to ATG8s strongly, with a preference for GABARAP, GABARAPL1 and GABARAPL2 (Figure 2 (D)). In reverse, His-GABARAP was pulled down strongly by GST-C1QBP, and slightly weaker by GST-CHCHD10 but not GST or GST-CHCHD2 (Figure 2(E)). His-GABARAPL1 (Figure 2F) and His-GABARAPL2 (Figure 2(G)) was pulled down strongly by GST-C1QBP, by GST-CHCHD10, very weakly by GST-CHCHD2 but not GST. This was consistent with Figure 2(B-D). Collectively, CHCHD2, CHCHD10 and C1QBP bound to ATG8s directly in vitro, with a preference for GABARAPs. Among CHCHD2, CHCHD10 and C1QBP, C1QBP bound to ATG8s most strongly, while CHCHD10 bound to ATG8s stronger than CHCHD2.

Potential binding motifs in CHCHD2-CHCHD10-C1QBP with ATG8

We mapped binding region(s) of ATG8s in CHCHD2, CHCHD10 and C1QBP. ATG8s bind to their targets via LC3-interacting Region (LIR) with a consensus sequence W/Y/F-x-x-L/I/V [70] (Figure 3(A)). CHCHD2 and CHCHD10 (151 and 142 aa) were predicted with 3 α-helices: α1 at the N terminus and α2-3 in 2 CX_9C motifs (CHCH domain) at the C terminus (Figure 3(C,E)) [71,72]. We identified a potential LIR region, 137FNEV140, in CHCHD2-α3 (Figure 3(A-C)), a potential LIR, 135YHGL138, immediately after CHCHD10-α3 (Figure 3(A,B,E)), and 2 potential LIRs in C1QBP (Figure 3(A,G)). We constructed and purified GST-CHCHD2, GST-CHCHD10 and GST-C1QBP mutants to pull down endogenous proteins in cell lysates (Figure 3(C-H)). CHCHD2 or CHCHD10 mutants, which lost a partial CHCH domain, were not as stable as their full-length protein when expressed in bacteria (Figure 3(D,F)).

GST-CHCHD2-WT, but not GST, pulled down endogenous CHCHD2, CHCHD10 and C1QBP and GABARAPL1 (Figure 3(C,D)). GST-CHCHD2^{Q126X}, lacking the potential LIR 137FNEV140, pulled down less GABARAPL1 than GST-CHCHD2-WT. However, GST-CHCHD2^{R145X}, with an intact potential LIR 137FNEV140, also pulled down less GABARAPL1 than GST-CHCHD2-WT (Figure 3(C,D)), suggesting the potential LIR of CHCHD2, 137FNEV140, did not contribute to CHCHD2-ATG8 interaction; instead, C-terminal 7 aa, 145–151 of CHCHD2, mediated CHCHD2-ATG8 interaction (Figure 3(B)). GST-CHCHD2^{G149X}, lacking the last 3 aa, bound to GABARAPL1, suggesting 145RLAN148 in CHCHD2, mediated CHCHD2-ATG8 interaction (Figure 3 (B-D)). 145RLAN148 was also important for CHCHD2 and CHCHD10 interaction (Figure 3(C,D)), suggesting ATG8 contributed to CHCHD2-CHCHD10 and CHCHD2-CHCHD2 interaction. Meanwhile, all CHCHD2 C-terminal truncation mutants pulled down C1QBP (Figure 3(C,D)),

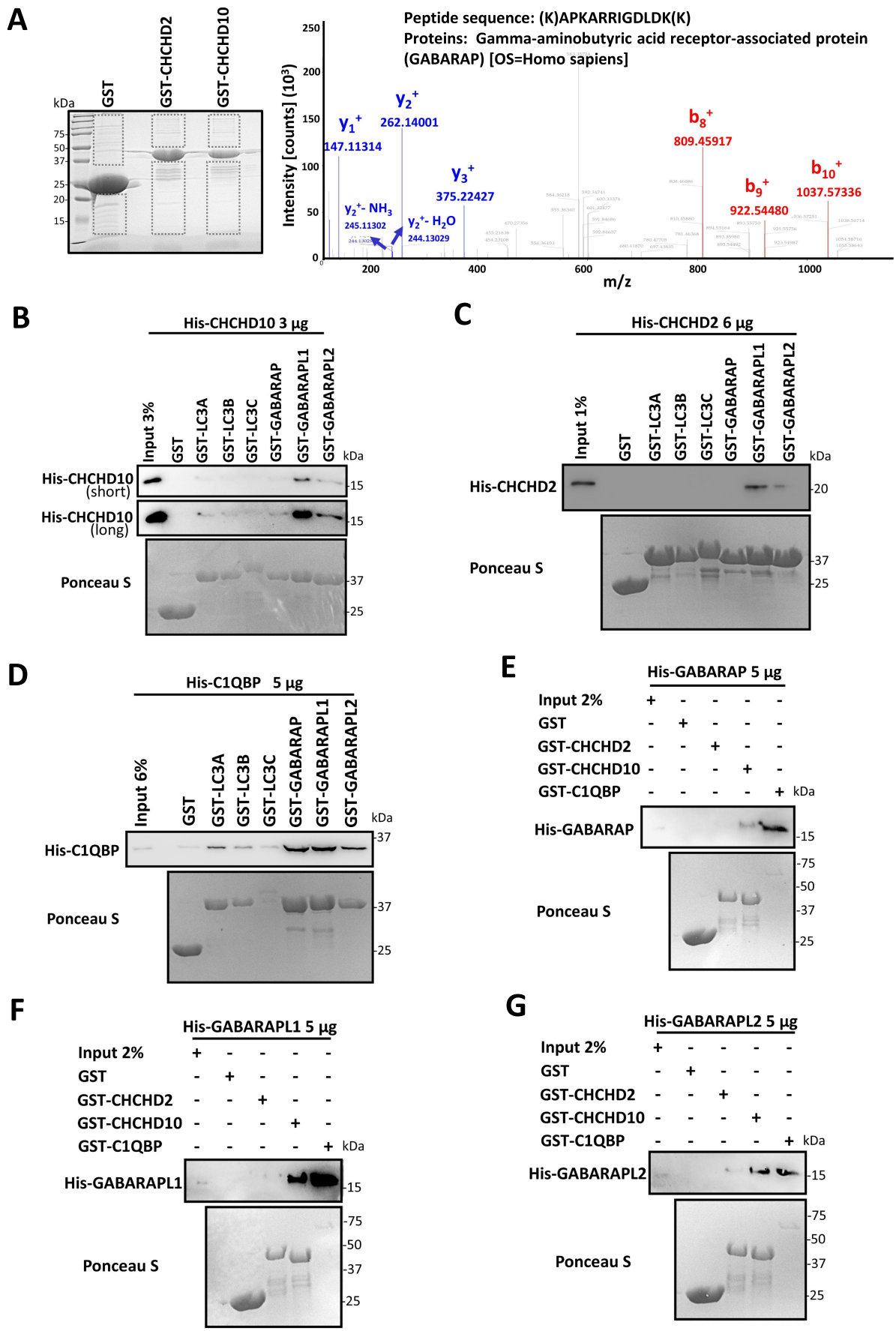

Figure 2. CHCHD2, CHCHD10 and C1QBP associated with ATG8s, individually. (A) GST, GST-CHCHD2 and GST-CHCHD10 pulled down SK-N-SH lysates. Proteins were separated in SDS-PAGE gel and subject to Coomassie Brilliant Blue staining. The protein gels were analyzed by LC-MS/MS. A peptide from GABARAP were identified. (B-D) His-CHCHD10 (B), His-CHCHD2 (C) and His-C1QBP (D) proteins pulled down by GST and GST-ATG8s. (E-G) His-GABARAP (E), His-GABARAPL1 (F) and His-GABARAPL2 (G) proteins pulled down by GST, GST-CHCHD2, GST-CHCHD10 and GST-C1QBP.

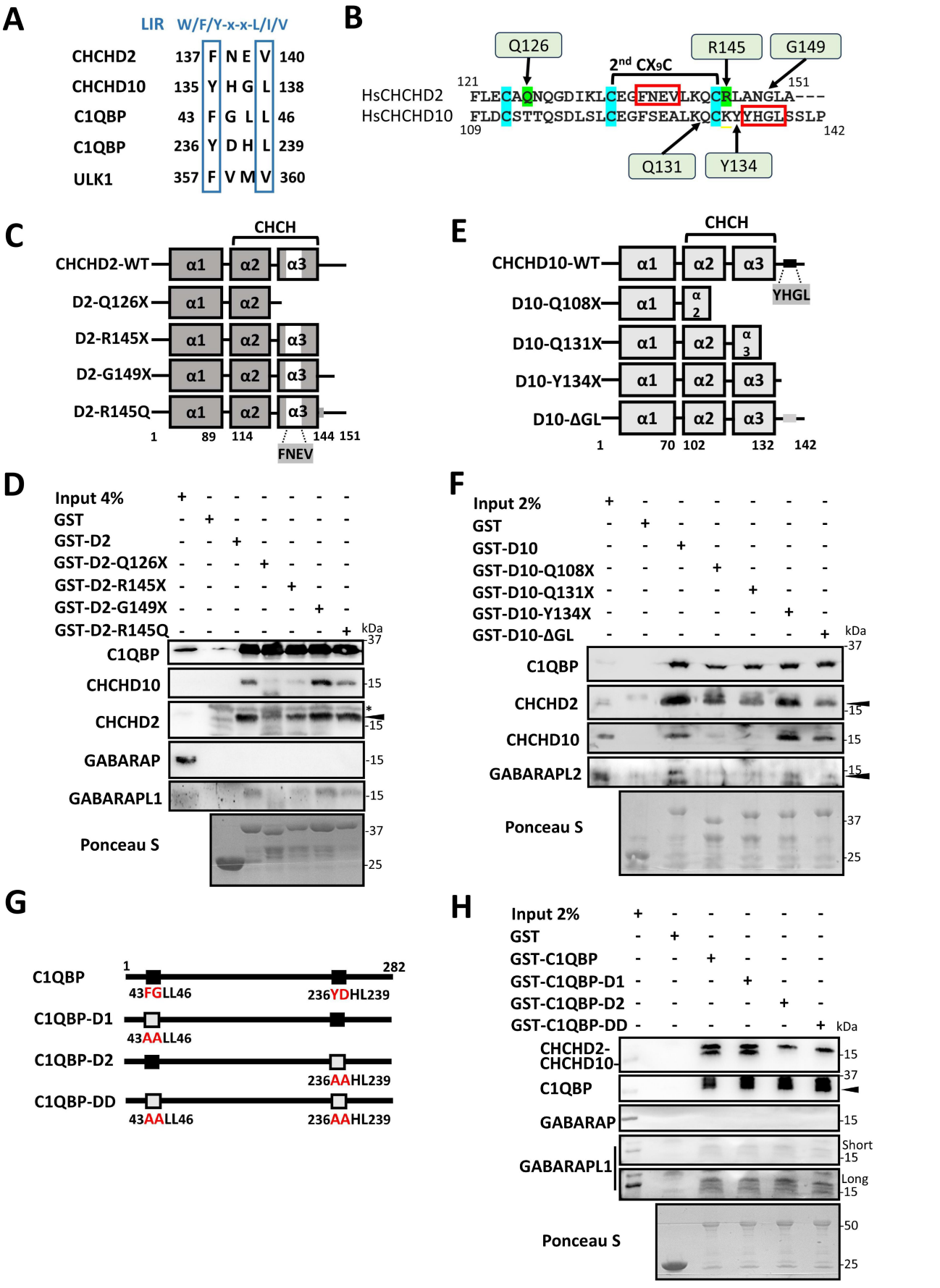

Figure 3. Potential ATG8 binding motifs were identified in CHCHD2, CHCHD10 and C1QBP. (A) Putative LC3-interacting motifs (LIRs) composing of canonical W/F/Y-x-x-L/I/V in CHCHD2, CHCHD10 and C1QBP, with a known LIR from ULK1. (B) Sequence of the C termini of CHCHD2 and CHCHD10. Conserved cysteine (C) in CX_9C motif was in blue. Amino acids involving in human patients were in green. The putative LIRs of CHCHD2 and CHCHD10, were labelled in red rectangles. Amino acids subjected to mutation were labelled. (C) Illustration of CHCHD2 mutations in 3 α-helices (α1, α2 and α3). α2-3 is the CHCH domain. The putative LIR,

suggesting the N terminus of CHCHD2 mediated CHCHD2-C1QBP interaction.

GST-CHCHD10-WT, but not GST, pulled down CHCHD2, CHCHD10, C1QBP and GABARAPL2 (Figure 3(E,F)). GST-CHCHD10^{Q108X} and GST-CHCHD10^{Q131X}, lacking most or half the of CHCH domain, lost substantial binding to CHCHD10 (Figure 3(B,E,F)), suggesting CHCH domain in CHCHD10 was essential for CHCHD10-CHCHD10 interaction. GST-CHCHD10^{Y134X}, lacking the last 8 aa including the potential LIR 135YHGL138 (Figure 3(B)), still pulled down CHCHD2 and CHCHD10, but reduced GABARAPL2 interaction (Figure 3(E,F)). GST-CHCHD10ΔGL, deleting 137GL138 in 135YHGL138, also reduced GABARAPL2 interaction, suggesting 135YHGL138 in CHCHD10 mediated CHCHD10-ATG8 interaction. Meanwhile, all CHCHD10 C-terminal truncation mutants pulled down C1QBP (Figure 3(E,F)), suggesting N-terminal CHCHD10 maintained C1QBP-CHCHD10 interaction.

GST-C1QBP pulled down endogenous CHCHD2, CHCHD10 and C1QBP. However, GST-C1QBP bound to little endogenous GABARAPL1 (Figure 3(G,H)), even with a strong C1QBP-GABARAPL1 interaction in vitro (Figure 2(F)). A possible explanation is that GABARAPL1 in lysates was not easily accessed by GST-C1QBP due to some steric hindrance. With little ATG8 pulled down by GST-C1QBP, it is hard to tell if potential LIRs of C1QBP contributed to C1QBP-ATG8 interaction (Figure 3(G,H)). Unexpectedly, C1QBP-D2 or C1QBP-DD, with mutations in 236YDHL239 of C1QBP, totally lost the binding of CHCHD10, but not CHCHD2 (Figure 3(G,H)), suggesting the 2nd potential LIR 236YDHL239 of C1QBP mediated C1QBP-CHCHD10 interaction.

Collectively, 145RLAN148 in CHCHD2 was important for CHCHD2-ATG8 interaction. 135YHGL138 in CHCHD10 contributed to CHCHD10-ATG8 interaction. 236YDHL239 in C1QBP contributed to C1QBP-CHCHD10 interaction. GST affinity-isolation assays revealed a large protein complex of CHCHD2-CHCHD10-C1QBP-ATG8s and suggested ATG8s were incorporated in CHCHD2-CHCHD10-C1QBP interaction. To comprehensively examine the assembly of CHCHD2-CHCHD10-C1QBP-ATG8 complex, we had to use in vitro protein-protein interaction assays.

Molecular architecture of CHCHD2-CHCHD10-C1QBP

We investigated how CHCHD2 and CHCHD10 bound to C1QBP and how CHCHD2 and CHCHD10 formed homo- or heterodimer. Based on Figure 3(C,E), we constructed and purified the N-terminal (α1) and C-terminal (α2–3) fragments of CHCHD2 (CHCHD2-N: 1–89 aa, CHCHD2-C: 90–151 aa) and CHCHD10 (CHCHD10-N: 1–82 aa, CHCHD10-C: 83–141 aa) (Figure 4(A)). Firstly, we investigated how CHCHD2 and CHCHD10 bound to C1QBP. His-C1QBP was bound to GST-CHCHD2-N, but not to GST-CHCHD2-C or GST (Figure 4(B)). Likewise, GST-CHCHD10-N, but not GST-CHCHD10-C or GST, bound to His-C1QBP (Figure 4(B)). Those data showed N termini of CHCHD2 and CHCHD10 bound to C1QBP, consistent with Figure 3(D,F).

We examined how CHCHD2 and CHCHD10 formed homo- or heterodimer. Protein dimer prediction algorithm PREDDIMER [73] suggested both N- and C-terminal CHCHD2 and CHCHD10 formed homo- or heterodimer (Figures S5E-F). GST-CHCHD2-N bound to His-CHCHD2 but not to GST-CHCHD2-C or GST (Figure S5G), suggesting CHCHD2 homodimer relied on its N terminus. GST-CHCHD2-C, but not GST-CHCHD2-N or GST, bound to His-CHCHD10 (Figure S5H), suggesting CHCHD2-CHCHD10 interaction was via the C terminus of CHCHD2. Both GST-CHCHD10-N and GST-CHCHD10-C bound to His-CHCHD2 weakly (Figure S5I). GST-CHCHD10-C bound to His-CHCHD10 stronger than GST-CHCHD10-N (Figure S5J), suggesting CHCHD10 homodimer mostly formed via C terminus of CHCHD10. Notably, CHCHD2 or CHCHD10 homo- or heterodimer interaction was much weaker than CHCHD2-C1QBP or CHCHD10-C1QBP interaction (Figure 4(B)), supporting C1QBP functioned as a scaffold to bring CHCHD2 and CHCHD10 together, and suggesting C1QBP promoted the formation of CHCHD2 or CHCHD10 dimer. There were CHCHD10 dimer and hints of tetramer pulled down by GST-C1QBP but not in input (Figure S5K), suggesting C1QBP promoted CHCHD10 dimer or oligomer formation (Figure S5L).

Molecular architecture of CHCHD2-CHCHD10-C1QBP with the ATG8 complex

We investigated how ATG8s incorporated into CHCHD2-CHCHD10-C1QBP complex. GST affinity-isolation assays using cell lysates suggested ATG8s bound to C terminus of CHCHD2 and CHCHD10 (Figure 3). By using purified proteins, both GST-CHCHD2-N and GST-CHCHD2-C, but not GST, bound to His-GABARAPL1 (Figure 4(C)) and His-GABARAPL2 (Figure 4(L)). Likewise, both GST-CHCHD10 -N and GST-CHCHD10-C, but not GST, bound to His-GABARAP (Figure 4(D)), His-GABARAPL1 (Figure S6A) and His-GABARAPL2 (Figure 4(E)), suggesting there could be 2 ATG8 molecules binding to N- and C-terminal

137FNEV140, is in α3. (D) GST, GST-CHCHD2 WT and GST-CHCHD2 mutants pulled down SK-N-SH lysates. Ponceau S staining showed the loading of GST proteins. *unspecific band. (E) Illustration of CHCHD10 mutations in 3 α-helices (α1, α2 and α3). α2–3 is the CHCH domain. The putative LIR, 135YHGL138, is after α3. D10-ΔGL, 137GL138 were deleted in 135YHGL138. (F) GST, GST-CHCHD10 WT and GST-CHCHD10 mutants pulled down HeLa lysates. (G) Illustration of putative LIRs and mutations in C1QBP. 43FGLL46 and 236YDHL239 were showed in black. C1QBP-D1, 43FGLL46 mutated to 43AALL46. C1QBP-D2, 236YDHL239 mutated to 236AAHL239. C1QBP-DD, double mutations 43AALL46 + 236AAHL239. (H) GST, GST-C1QBP WT and GST-C1QBP mutants pulled down SK-N-SH lysates.

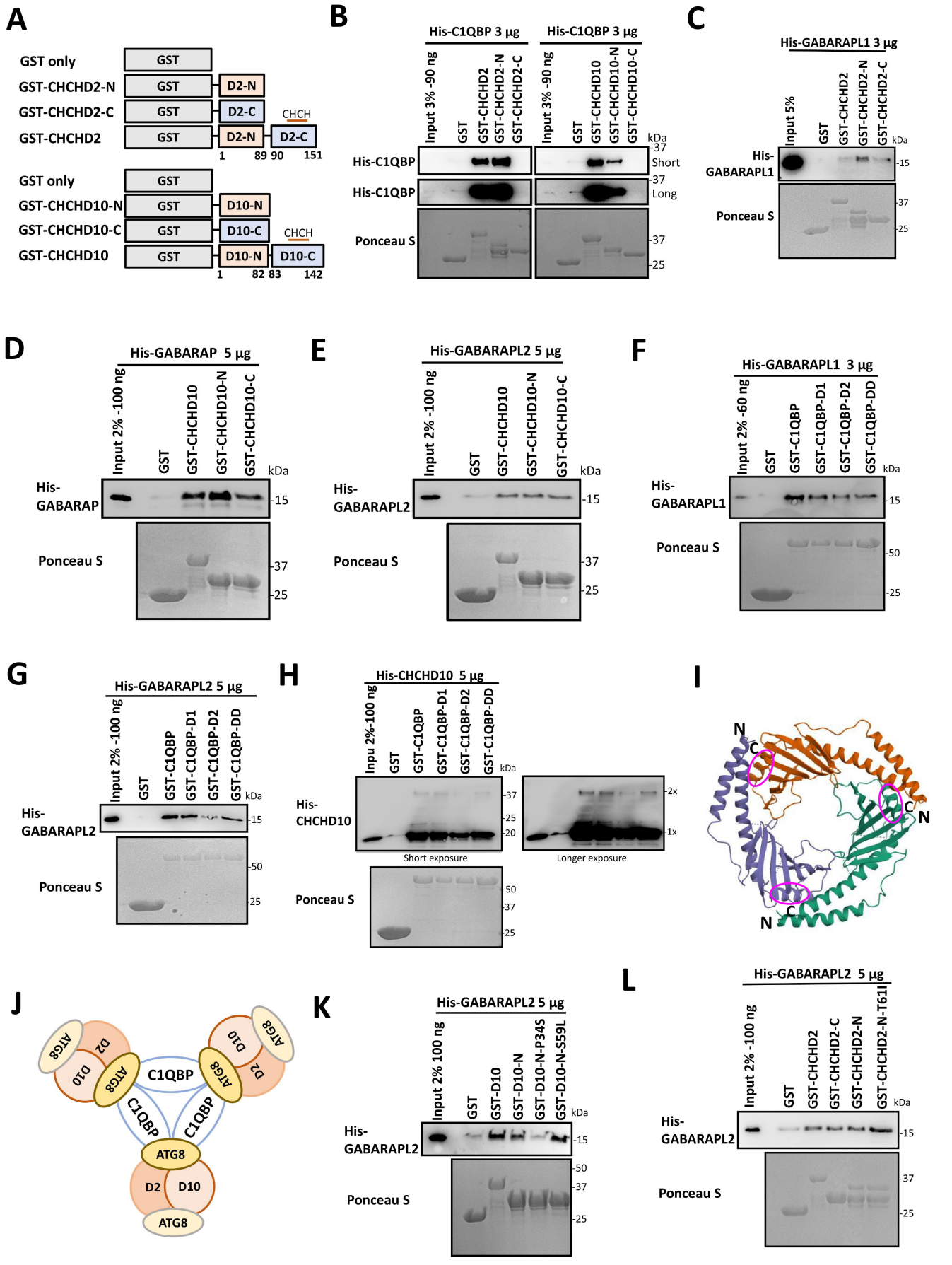

Figure 4. ATG8s assembled in CHCHD2-CHCHD10-C1QBP complex. (A) Illustration of GST-CHCHD2 and GST-CHCHD10 fragments. CHCHD2-N and CHCHD10-N contain α1. CHCHD2-C and CHCHD10-C contain α2 and α3. (B) In vitro affinity isolation of His-C1QBP protein by GST, GST-CHCHD2, GST-CHCHD2-N (1-89) and GST-CHCHD2-C (90-151) proteins, or by GST, GST-CHCHD10, GST-CHCHD10-N (1-82) and GST-CHCHD10-C (83-142) proteins. (C) In vitro affinity isolation of His-GABARAPL1 by GST,

CHCHD2 or CHCHD10 simultaneously. However, there is no predicted LIR in the N terminus of CHCHD2 or CHCHD10 but only one in the C terminus (Figure 3(A)). A potential homo- or heterodimer interface [74] formed by the N termini of CHCHD2 and CHCHD10 when binding to C1QBP, could mediate the interaction between the N-terminal CHCHD2 and CHCHD10 with ATG8s.

We tested how ATG8s bound to C1QBP in vitro. Mutations in potential LIRs in C1QBP, C1QBP-D2 (236AAHL239), and C1QBP-DD (43AALL46 + 236AAHL239), showed reduced binding to His-GABARAPL1 (Figure 4(F)), His-GABARAPL2 (Figure 4(G)), and His-GABARAP (Figure S6B), suggesting both putative LIRs in C1QBP mediated C1QBP-ATG8 interaction, and the 2nd LIR, 236YDHL239, contributed more. All C1QBP mutants (C1QBP-D1, C1QBP-D2 and C1QBP-DD) did not change C1QBP-CHCHD2 interaction (Figure S6C), but C1QBP-D2 pulled down less CHCHD10 monomer or dimer (Figure 4(H)). Such results suggested C1QBP 236YDHL239 facilitated both CHCHD10-C1QBP and ATG8-C1QBP interaction, i.e. CHCHD10 binding site in C1QBP overlapped with or was adjacent to ATG8 binding sites in C1QBP. X-ray crystal structure of C1QBP protein (74-282 aa including 2nd LIR motif 236YDHL239) showed a C1QBP trimer (Figure 4(I)) in which 1-73 aa, including 1st LIR motif 43FGLL46, was unstructured [69]. 236YDHL239 in C1QBP, the binding site for CHCHD10 and ATG8, is at the edge of prism of C1QBP trimer (Figure 4(I)). Collectively, N termini of CHCHD2 and CHCHD10 with ATG8s bound to C1QBP, while C termini of CHCHD2 and CHCHD10 could bind another ATG8s (Figure 4(J)).

Many neurodegeneration-causing CHCHD2 or CHCHD10 mutations are located at N-terminal α1 (Figure 3(C,E)) [63,72]. We asked whether those mutations affected protein-protein interactions. We constructed and purified GST-CHCHD2-N^{T61I} based on GST-CHCHD2-N (Figure 4(A)), GST-CHCHD10-N^{P34S} and GST-CHCHD10-N^{S59L} using GST-CHCHD10-N (Figure 4(A)). GST-CHCHD2-N and GST-CHCHD2-N^{T61I} bound to His-C1QBP with similar affinity (Figure S6D). GST-CHCHD10-N, GST-CHCHD10-N^{P34S} and GST-CHCHD10-N^{S59L} bound to His-C1QBP with similar affinity (Figure S6E). Compared to GST-CHCHD10-N, GST-CHCHD10-N^{P34S} bound less to His-GABARAPL2, while GST-CHCHD10-N^{S59L} bound more to His-GABARAPL2 (Figure 4(K)). Compared to GST-CHCHD2-N, GST-CHCHD2-N^{T61I} showed enhanced binding to His-GABARAPL2 (Figure 4(L)). Collectively, N-terminal disease-causing CHCHD2 or CHCHD10 mutants indeed varied ATG8 interaction but did not disrupt CHCHD2-CHCHD10-C1QBP-ATG8 complex as they still bound to C1QBP via the N terminus, and to CHCHD10 and CHCHD2 via the C terminus.

CHCHD2 and CHCHD10 were degraded via ATG8s

CHCHD2, CHCHD10 and C1QBP protein are enriched in mitochondria but can also be present in the cytosol. ATG8s are present mostly in the cytosol and sometimes in mitochondria [75]. We wondered if there was colocalization of CHCHD2 and CHCHD10 with ATG8s and the biological consequence of such interaction. We overexpressed GFP-GABARAPL1 with CHCHD2, CHCHD10 or C1QBP. GFP-GABARAPL1 was cytosolic forming puncta. CHCHD2, CHCHD10 or C1QBP was near GFP-GABARAPL1 puncta (Figure 5(A-C)). Endogenous CHCHD2, CHCHD10 or C1QBP showed similarly, near GFP-GABARAPL1 puncta (Figure S7A). CHCHD2 and CHCHD10 located alongside overexpressed GFP-GABARAP or GABARAPL2 puncta, colocalizing with lysosomal marker LAMP1 (Figures S7B-G), suggesting CHCHD2 and CHCHD10 underwent degradation via GABARAPs. To test this, we overexpressed GFP-GABARAPs. Endogenous CHCHD2 and CHCHD10 were reduced upon GABARAPs expression, and such reduction was inhibited by lysosome inhibitor bafA1 (Figure 5(D)), suggesting GABARAPs degraded CHCHD2 and CHCHD10 via lysosomes. As CHCHD2 and CHCHD10 decayed fast (Figure 1(A)), we wondered if the decay of CHCHD2 and CHCHD10 could be slowed down if they bound less to GABARAPs via their C termini. CHCHD2^{R145Q} or CHCHD10ΔGL, with reduced ATG8 binding (Figure 3(D,F)), decayed slower than their WT (Figure 5(E,F)). We also tested other disease-associated CHCHD2 and CHCHD10 mutants. CHCHD2^{T61I}, CHCHD10^{S59L} and CHCHD10^{G58R}, all showed an enhanced half-life compared to their WT (Figures S7H-I). To further investigate the autophagic degradation of CHCHD2 and CHCHD10, we transiently knocked down *ATG5* (autophagy related 5) or *ATG7*, two key players in canonical lipid conjugation machinery of macroautophagy [76]. CHCHD2 or CHCHD10 was either unchanged or reduced upon *ATG5* or *ATG7* knockdown (Figure 5(G)), suggesting ATG5- or ATG7-mediated ATG8 lipidation may not be required for the autophagic degradation of CHCHD2 or CHCHD10. CHX (cycloheximide)-based protein turnover assay also showed *ATG5* or *ATG7* knockdown did not reduce the degradation rate of CHCHD2 or CHCHD10 (Figure S7J). Collectively, GABARAPs bound to CHCHD2 and CHCHD10, caused ATG5- and ATG7-independent autophagic degradation of CHCHD2 and CHCHD10.

PD-linked CHCHD2^{T61I} forms aggregates [47,77]. As CHCHD2^{T61I} binds to ATG8s, we wondered if CHCHD2^{T61I} was present in lysosomes. We constructed CRISPR (clustered regularly interspaced short palindromic repeats)-edited *CHCHD2*$^{-/-}$ and *CHCHD2*^{T61I} hESCs (human embryonic stem

GST-CHCHD2, GST-CHCHD2-N and GST-CHCHD2-C. (D-E) In vitro affinity isolation of His-GABARAP (D) and His-GABARAPL2 (E) by GST, GST-CHCHD10, GST-CHCHD10-N and GST-CHCHD10-C. (F-H) in vitro affinity isolation of His-GABARAPL1 (F), His-GABARAPL2 (G), His-CHCHD10 (H) by GST-C1QBP WT or mutants, as illustrated in Figure 3G. (I) The illustration of the 2nd LIRs in crystal structure of C1QBP (74-282 aa). PDB ID code: 1p32. Pink circles, LIR 236YDHL239. (J) Schematic illustration of CHCHD2-CHCHD10-C1QBP-ATG8 complex. ATG8 bound to the edge of C1QBP trimer. CHCHD10 bound to the same or nearby region. Another ATG8, bound to C termini of CHCHD2 and CHCHD10. D2, CHCHD2; D10, CHCHD10. (K-L) In vitro affinity isolation of His-GABARAPL2 proteins by GST-CHCHD10, GST-CHCHD10-N. GST-CHCHD10-N^{P34S}, GST-CHCHD10-N^{S59L} (K) or GST-CHCHD2, GST-CHCHD2-C, GST-CHCHD2-N and GST-CHCHD2-N^{T61I} (L).

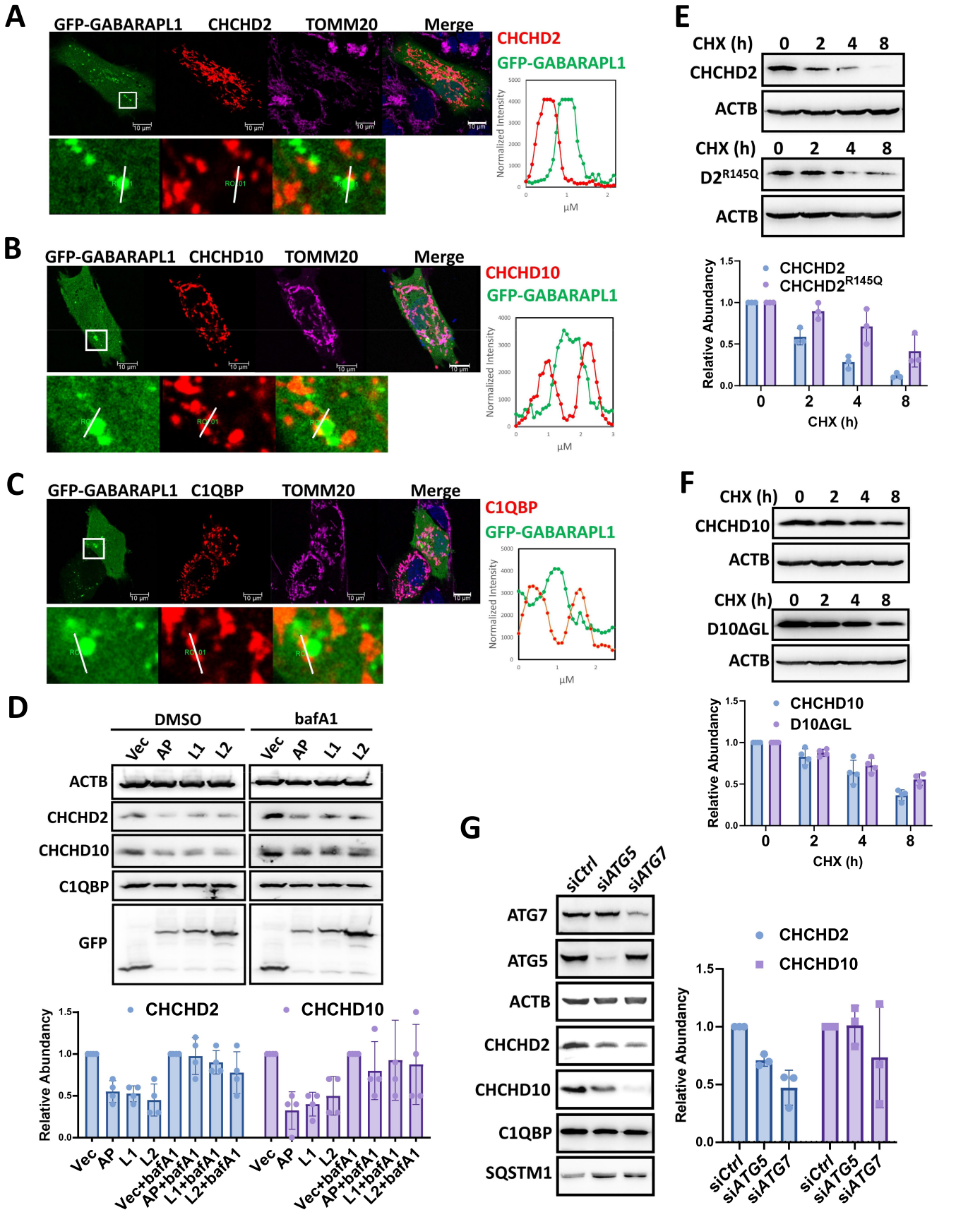

Figure 5. CHCHD2 and CHCHD10 were degraded via ATG8s. (A-C) Confocal imaging of GFP-GABARAPL1 with CHCHD2-FLAG-MYC (red) (A), CHCHD10-FLAG-MYC (red) (B), C1QBP-FLAG-MYC (red) (C) and TOMM20 (purple) in SK-N-SH cells. Scale bar: 10 μm. (D) Western blot analysis on HeLa cells transfected with GFP-GABARAPs for 24 h. Cells were treated with 200 ng/ml bafA1 for 5 h. Vec, GFP vector; AP, GFP-GABARAP; L1, GFP-GABARAPL1; L2, GFP-GABARAPL2. Quantification of CHCHD2 and CHCHD10 normalized with ACTB. $n = 4$. (E) Western blot analysis on SK-N-SH cells transfected with non-tagged-CHCHD2-WT or CHCHD2^{R145Q} followed by 50 μg/ml CHX treatment. Quantification of CHCHD2 normalized with ACTB were shown. $n = 3$. (F) Western blot analysis on SK-N-SH cells transfected with non-tagged-CHCHD10 -WT or CHCHD10ΔGL followed by 50 μg/ml CHX treatment. Quantification of CHCHD10 normalized with ACTB were shown. $n = 4$. (G) Western blot analysis on transient knockdown of *ATG5* or *ATG7* for 48 h in SK-N-SH cells. Quantification of CHCHD2 normalized with ACTB was shown. $n = 3$.

cells) and generated human midbrain-like organoids (hMLOs) from those lines (Figures S8A-B). These hMLOs contained MAP2-positive neurons with midbrain dopaminergic (DA) neuron identity (TH [tyrosine hydroxylase]), NR4A2/NURR1, PITX3) with no gross defects (Figures S8C-D). In CRISPR-edited *CHCHD2*^{T61I} DA neurons, CHCHD2^{T61I} colocalized with lysosome marker LAMP1 (Figure S8E). However, when transiently overexpressed in cells, CHCHD2^{T61I}, similar as CHCHD2 WT, was adjacent to the puncta of GFP-GABARAPL1 and LAMP1 but did not colocalize with LAMP1 (Figure S8F), suggesting CHCHD2^{T61I} colocalizing with lysosomes only occurred under chronic conditions, but not transiently. Moreover, transient overexpression of CHCHD2^{T61I}, but not CHCHD2 WT, led to protein aggregates shown by PROTEOSTAT® Dye (a commercially available protein aggregation assay) staining under the treatment of lysosome inhibitor bafA1 but not dimethyl sulfoxide (DMSO) (Figure S8G). Similar results on CHCHD10 WT and CHCHD10^{S59L} were observed (Figures S8H-I), suggesting protein aggregates caused by CHCHD2 or CHCHD10 mutants build up over time or under environmental stress such as inhibition of lysosomes.

CHCHD2 and CHCHD10 recruited ULK1 via ATG8s

ATG8 forms the central axis of autophagy by binding many autophagy proteins. We hypothesized GABARAPs, binding to the C termini of CHCHD2 and CHCHD10, may recruit some other ATG8-binding proteins (Figure 4(J)). GST affinity-isolation assay showed GST-CHCHD2 and GST-CHCHD10, but not GST, pulled down ULK1 (unc-51 like kinase 1), a master kinase of autophagy initiation [78] (Figure 6(A)). Bacterial-expressed C1QBP, however, did not pull down ULK1 (Figure 6(A)), even it pulled down CHCHD2 and CHCHD10 strongly (Figure 3(H)). ULK1 complexes with RB1CC1/FIP200 (RB1-inducible coiled-coil 1), ATG13 (autophagy related 13) and ATG101 to initiate autophagy [78]. RB1CC1 was pulled down by GST-CHCHD10 (Figure 6(A)), while ATG13 or ATG101 was not (Figure 6(A)). Co-immunoprecipitation assay showed ULK1 pulled down a small portion of endogenous CHCHD2 and CHCHD10, but little C1QBP (Figure 6(B)). RB1CC1 pulled down ATG13, some CHCHD2, hints of CHCHD10 and C1QBP (Figure S9A). Reverse co-immunoprecipitation assay showed CHCHD2, however, bound to little ULK1 or RB1CC1 even it strongly interacted with CHCHD10, CHCHD2 and C1QBP (Figure 6B). Similarly, CHCHD10 pulled down little ULK1 or RB1CC1 (Figure S9B).

To confirm CHCHD2-CHCHD10-ULK1 interaction was mediated by ATG8s bound to the C termini of CHCHD2 and CHCHD10, we carried out GST affinity-isolation assay with CHCHD2 or CHCHD10 mutants. CHCHD2^{Q126X} or CHCHD2^{R145Q} which reduced ATG8 binding (Figure 3(D)), lost or reduced ULK1 interaction but still bound to C1QBP (Figure 6(C)). CHCHD10^{Q108X} or CHCHD10^{Q131X}, C-terminal truncation mutations of CHCHD10 losing most ATG8 binding (Figure 3(F)), cannot pull down ULK1 (Figure 6(D)) but still bound to C1QBP. Those results evidenced CHCHD2-CHCHD10-ULK1 interaction was mediated by ATG8s bound to CHCHD2 or CHCHD10 but not C1QBP.

We investigated if CHCHD2, CHCHD10 and C1QBP colocalized with ULK1. HA-ULK1 showed little colocalization with mitochondrial CHCHD2, CHCHD10 and C1QBP, but torin1 treatment caused some ULK1 signal overlapping with CHCHD2, CHCHD10 or C1QBP (Figure 6(E)), suggesting CHCHD2-CHCHD10-ULK1 interaction could be regulated by upstream signals. Overexpression of GFP-GABARAPL1, HA-ULK1 with CHCHD2 or CHCHD10 showed GFP-GABARAPL1 and HA-ULK1 were in adjacent puncta while CHCHD2 or CHCHD10 was absent from GFP-GABARAPL1 and HA-ULK1 signal (Figures S9C-F), consistent with Figure 5. As ULK1 initiates autophagy, we asked if ULK1 promoted degradation of CHCHD2 or CHCHD10. Overexpression of ULK1 or kinase-dead ULK1^{K46N} [79], did not change CHCHD2 or CHCHD10 (Figure 6(F)). ULK1 activator BL-918 or ULK1 inhibitor SBI-0206965 did not change CHCHD2 or CHCHD10 as expected (Figure 6(G)), suggesting some other ATG8 binding proteins but not ULK1, degrade CHCHD2 and CHCHD10.

CHCHD2 and CHCHD10 promoted autophagy

ULK1-GABARAPs interaction promotes autophagy, while ULK1-MAP1LC3s interaction inhibits autophagy [80]. With CHCHD2 and CHCHD10 preferentially interacting with GABARAPs and ULK1, we asked if CHCHD2 and CHCHD10 promoted autophagy. We carried out an autophagy flux assay. CHCHD2 knockdown enhanced SQSTM1/p62 (sequestosome 1). si*CHCHD2* reduced MAP1LC3-II upon EBSS compared to si*Ctrl*, suggestive of a blocked autophagy flux (Figure 7(A)). We monitored the puncta formation of endogenous ATG13 upon autophagy initiation by EBSS upon *CHCHD2* knockdown. ATG13 formed puncta upon EBSS treatment, an indicative of autophagosome formation (Figure 7(B)). However, ATG13 failed to form puncta in *CHCHD2*-knockdown cells upon EBSS, suggestive of impairment of autophagy initiation. Similar results were seen in cells transfected with si*CHCHD2* with exogenous HA-ATG13 (Figure S9G). To test this in neurons, we used *CHCHD2*^{T61I} and *CHCHD2*$^{-/-}$ DA neurons derived from iPSCs (Figures S8C-D). We monitored the puncta formation of endogenous WIPI2 (WD repeat domain, phosphoinositide interacting 2) upon autophagy activation by torin1. Torin1 induced more WIPI2 puncta in WT DA neurons but failed to do so in *CHCHD2*^{T61I} or *CHCHD2*$^{-/-}$ neurons (Figure 7(C)), indicating autophagic defects in *CHCHD2*^{T61I} and *CHCHD2*$^{-/-}$ neurons. To further validate this, we carried out an autophagy flux assay on isogenic ESCs. Torin1 enhanced the autophagy flux in cells carrying WT CHCHD2 but failed to do so in cells carrying CHCHD2^{T61I} or without CHCHD2 (Figure 7(D)). This result corroborated with Figure 7(C) to show autophagy defects in *CHCHD2*^{T61I} and *CHCHD2*$^{-/-}$ cells.

T61I locates at the N terminus of CHCHD2, but CHCHD2 recruited ULK1 via its C terminus (Figure 6(C)), suggesting T61I in CHCHD2 did not directly interfere with CHCHD2-ULK1 interaction. GST-CHCHD2-N^{T61I} (N-terminal fragment) showed stronger binding to

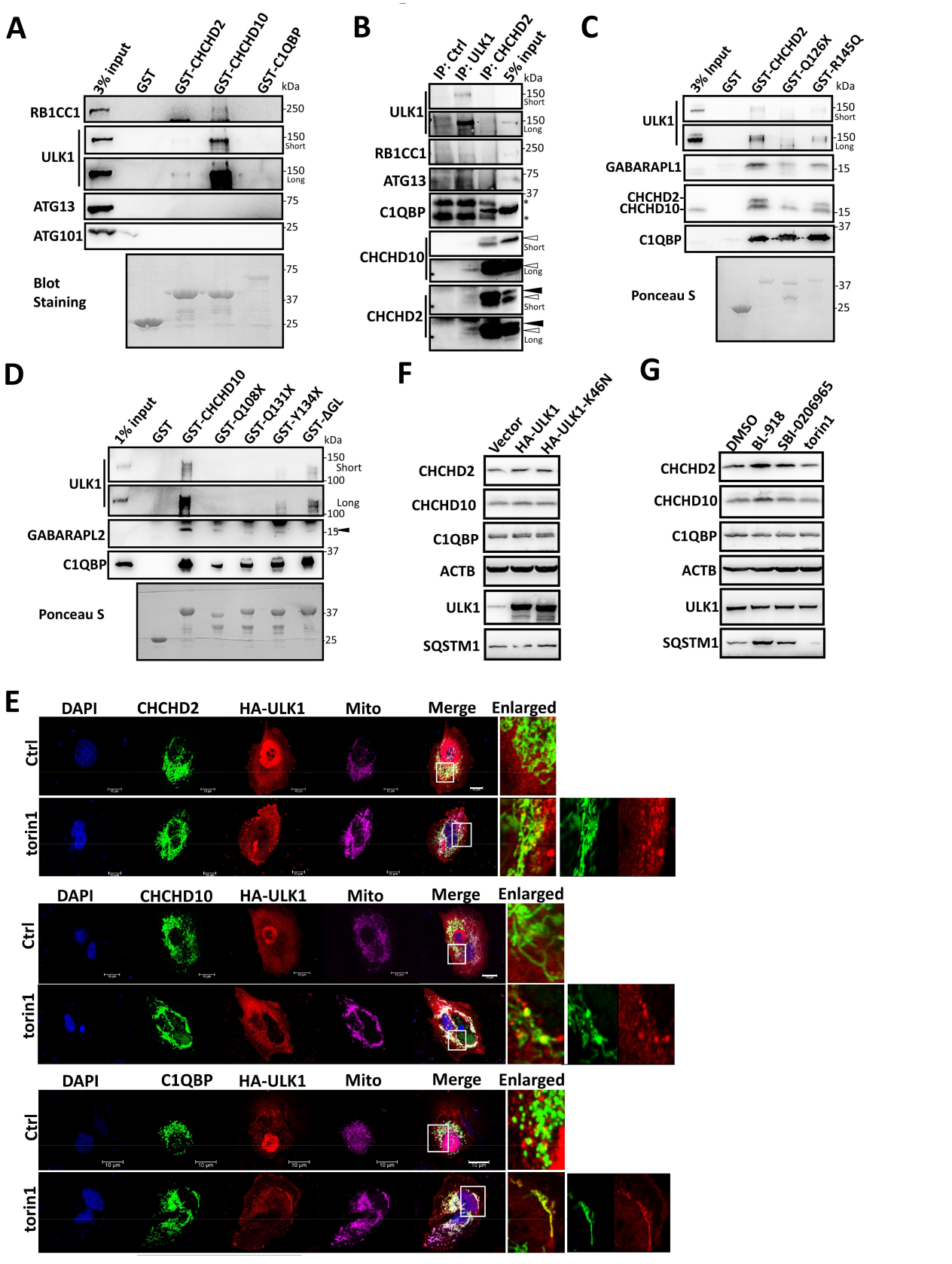

Figure 6. CHCHD2 and CHCHD10 recruited ULK1 complex via ATG8s. (A) GST, GST-CHCHD2, GST-CHCHD10 and GST-C1QBP pulled down SK-N-SH lysates. (B) Co-immunoprecipitation of endogenous proteins by antibodies against ULK1 or CHCHD2 in SK-N-SH cells. Open arrow, CHCHD10. Black arrow, CHCHD2. *unspecific band. (C-D) GST, GST-CHCHD2-WT and GST-CHCHD2 mutants (C) or GST, GST-CHCHD10 WT and GST-CHCHD10 mutants (D) pulled down SK-N-SH lysates. (E) Confocal imaging of CHCHD2-FLAG-MYC, CHCHD10-FLAG-MYC, or C1QBP-FLAG-MYC (green), HA-ULK1 (red) upon 250 nM torin1 for 3 h. Mito, MitoTracker™ Deep red. Scale bar: 10 μm. (F) Western blot analysis on SK-N-SH cells with overexpression of HA-ULK1 or HA-ULK1^{K46N} for 24 h. (G) Western blot analysis on SK-N-SH cells treated with ULK1 activator BL-918 5 μM or ULK1 inhibitor SBI-0206965 10 μM for 24 h.

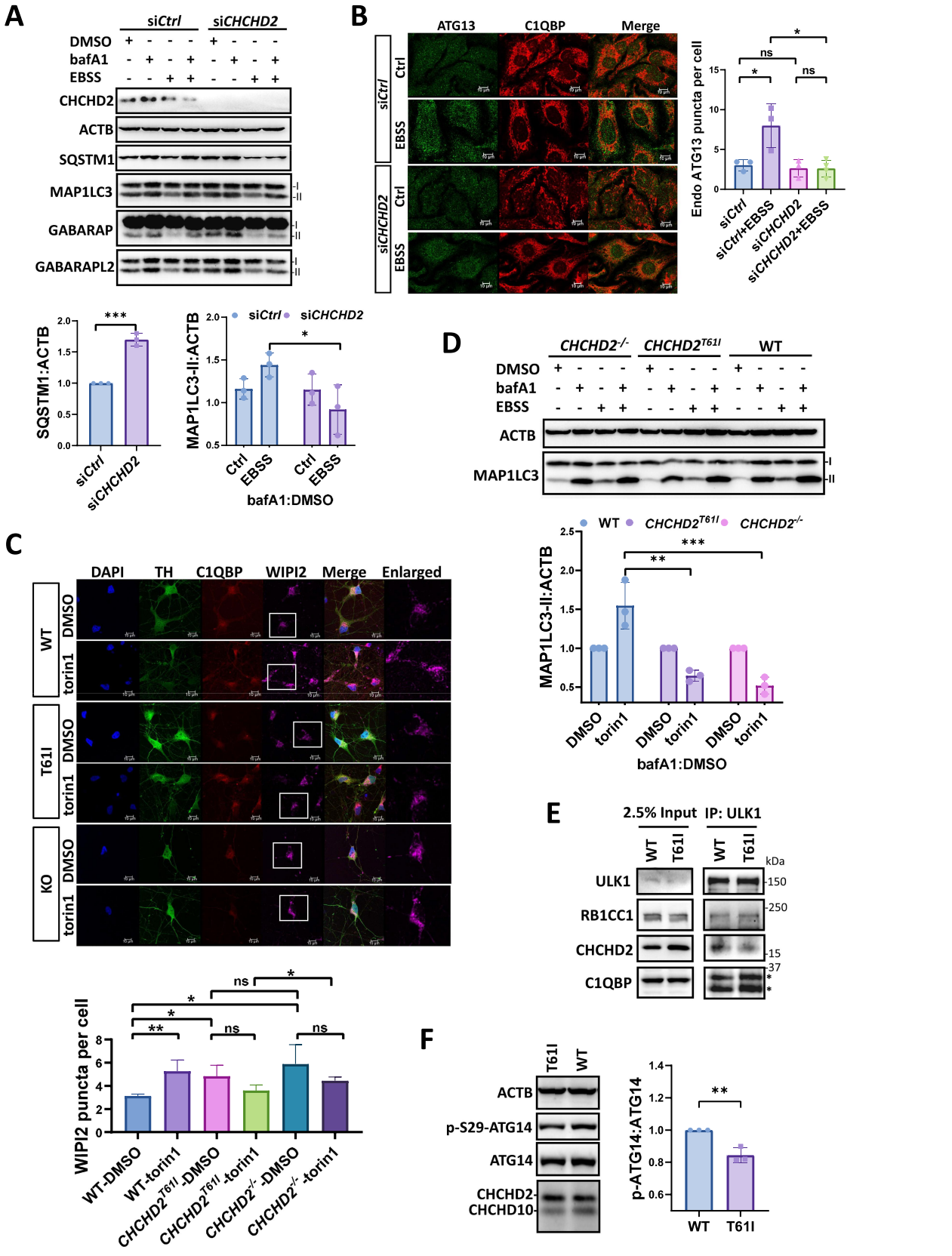

Figure 7. CHCHD2 promoted autophagy. (A) Autophagy flux assay on HeLa cells with 48 h transfection of si*Control* or si*CHCHD2*. Cells were then treated with DMSO, bafA1, EBSS or bafA1+ EBSS for 2 h. SQSTM1/p62 and MAP1LC3-II levels were quantified by densitometry and plotted as mean ± S.D. of 3 independent experiments. Lower left: quantification of SQSTM1:ACTB. Unpaired t test, ***$p = 0.0003$. Lower right: quantification of MAP1LC3-II:ACTB. Ctrl refers to the basal change of bafA1: DMSO. EBSS refers to the change of bafA1:DMSO upon autophagy activation by EBSS. 2-way ANOVA, *$p = 0.0454$ (si*Ctrl* vs si*CHCHD2*). (B) Confocal imaging of HeLa cells transiently transfected with si*Control* or si*CHCHD2* for 48 h. Cells were then treated with EBSS for 5 h. Endogenous ATG13 or C1QBP was labelled with green or red. Scale bar: 10 μm. Quantification of puncta formed by ATG13. n ~ 100 cells per group. Unpaired t test, ns, $p = 0.6418$ (si*Ctrl* vs si*CHCHD2*); *$p = 0.0152$ (si*Ctrl*+EBSS

GABARAPL2 (Figure 4(L)) in vitro, suggesting CHCHD2^{T61I} may make CHCHD2-CHCHD10-C1QBP-ATG8 complex tighter, therefore indirectly affected CHCHD2-ULK1 interaction. With iPSC-derived *CHCHD2*^{T61I} dopaminergic neurons and hESCs exhibiting impaired autophagy initiation (Figure 7(C,D)), we wondered how CHCHD2^{T61I} affected its interaction with ULK1. To test this, we used in vitro-purified GST-CHCHD2 and GST-CHCHD2^{T61I} (full length) protein to affinity-isolate components from cell lysates. GST-CHCHD2^{T61I} did not impair CHCHD2-ULK1 interaction compared with GST-CHCHD2 as expected (Figure S9H). We then monitored CHCHD2-ULK1 interaction in isogenic hESCs carrying CHCHD2 or CHCHD2^{T61I} by using ULK1 antibody to pull down endogenous proteins (Figure 7(E)). Some reduction of CHCHD2-ULK1 interaction was seen in CHCHD2^{T61I} line compared with CHCHD2 WT, suggesting an impairment of CHCHD2-ULK1 interaction caused by CHCHD2^{T61I} in cells. ULK1 phosphorylates ATG14 (autophagy related 14) at Ser29 during autophagy. Phospho-ATG14 (Ser29) normalized with total ATG14 was reduced in cells carrying CHCHD2^{T61I} compared with WT, suggesting of a reduction of ULK1 activity in *CHCHD2*^{T61I} line (Figure 7(F)). Collectively, CHCHD2^{T61I} slightly reduced CHCHD2-ULK1 interaction in cells, which could explain autophagic defects seen in cells carrying CHCHD2^{T61I}.

Transiently overexpressed C-terminal FLAG-MYC-tagged CHCHD2, CHCHD10 or C1QBP reduced autophagy substrate SQSTM1 (Figure 8(A)). Overexpressed non-tagged CHCHD2 also reduced SQSTM1 and enhanced phospho-BECN/Beclin1 (Ser30) (Figure 8(B)), suggestive of autophagy activation, whereas MAP1LC3-II changed little. Overexpressed non-tagged CHCHD10 also reduced SQSTM1 (Figure 8(C)). When transiently overexpressing CHCHD2 or CHCHD10 mutants, endogenous SQSTM1 was also reduced (Figure 8(B,C)). mCherry-ZFYVE1 /DFCP1 (zinc finger FYVE-type containing 1) marks the formation of precursor of autophagosome, which forms puncta upon autophagy activation [81]. When co-overexpressing mCherry-ZFYVE1 with CHCHD2, CHCHD10 or C1QBP, some colocalization of mCherry-ZFYVE1 with CHCHD2 was observed. More mCherry-ZFYVE1 puncta were formed with overexpression of CHCHD2, CHCHD10 or C1QBP than control (Figure S9I). To corroborate the above finding, we constructed an autophagy reporter HeLa cell line expressing GFP-LC3-RFP-LC3ΔG [82]. Autophagic flux can be estimated by calculating the GFP:RFP signal ratio, when the probe is cleaved by endogenous ATG4 proteases into equimolar amounts of GFP-LC3 and RFP-LC3ΔG. GFP-LC3 is degraded by autophagy, while RFP-LC3ΔG remains in the cytosol, serving as an internal control (Figure S9J). Using this probe, we found transiently overexpressed CHCHD2, CHCHD10 or C1QBP reduced GFP:RFP ratio, indicating an activation of autophagy. *CHCHD2* knockdown enhanced GFP:RFP ratio, suggesting a blockage of autophagy-lysosome pathway (Figures S9K-L). Collectively, CHCHD2 and CHCHD10 promoted autophagosome formation and reduced SQSTM1. Impaired autophagy initiation was seen upon transient *CHCHD2* knockdown and in *CHCHD2*^{T61I} or *CHCHD2*$^{-/-}$ DA neurons, pointing to a positive role of CHCHD2 in autophagy.

CHCHD2 promoted protein aggregate clearance

CHCHD2 and CHCHD10 mutations caused protein aggregates. With CHCHD2 and CHCHD10 promoting autophagy, we asked if CHCHD2 and CHCHD10 played a role in protein aggregate clearance. Transient puromycin treatment causes intracellular protein aggregates marked with UB, while no aggregates were observed in control cells [83,84]. Puromycin caused significantly more UB-positive puncta in cells transfected with si*CHCHD2*, si*CHCHD10* or si*C1QBP* than si*Ctrl* (Figure 8(D)). A reduced CHCHD2 signal reflected the positive transfection of siRNAs because si*CHCHD2*, si*CHCHD10* or si*C1QBP* decreased endogenous CHCHD2 (Figure S9M). This result suggested CHCHD2, CHCHD10 and C1QBP may help to clear intracellular protein aggregates. Some UB-positive puncta colocalized with endogenous CHCHD2 (Figure 8(D)). We then asked if CHCHD2 promoted degradation of pathological aggregates. Co-overexpression of CHCHD2, CHCHD10 or C1QBP in HeLa cells reduced delivered MAPT/Tau (microtubule associated protein tau) aggregates (Figure 8(E)) and aggregation-prone FUS^{P525L} (FUS RNA binding protein) in the insoluble fractions (Figure 8(F)). SNCA/α-synuclein pre-formed fibril (PFF) delivered to cells formed SNCA aggregates, reflected as SNCA in the insoluble fraction [85]. Transiently overexpressed CHCHD2 reduced SNCA in the insoluble fraction in HeLa cells (Figure 8(G)), suggesting CHCHD2 reduced SNCA aggregates. We also used a stable GFP-SNCA^{A53T} overexpressed HeLa line to see if CHCHD2 located near SNCA aggregates. When PFF was introduced, cytosolic GFP-SNCA^{A53T} forms aggregates as green dots. Overexpressed CHCHD2, CHCHD10 or C1QBP located besides SNCA aggregates (Figure S9N). Lastly, we asked if CHCHD2 reduced protein aggregates in vivo. We used a mouse model with PFF injected in the striatum with control or CHCHD2 virus (Figure 8(H)). In PFF-injected mice, SNCA

vs si*CHCHD2*+EBSS); *$p = 0.0401$ (si*Ctrl* vs si*Ctrl*+EBSS); ns, $p = 0.9768$ (si*CHCHD2* vs si*CHCHD2*+EBSS). (C) Confocal imaging of dopaminergic neurons at day 60 derived from WT (H9), *CHCHD2*^{T61I} and *CHCHD2*$^{-/-}$ lines. Neurons were treated with torin1 250 nM for 5 h. TH, tyrosine hydroxylase. Endogenous C1QBP and WIPI2 labelled as red and far-red. Scale bar: 10 µm. Quantification of puncta formed by WIPI2. n ~ 100 cells per group. Unpaired t test, WT-DMSO vs WT-torin1, **$p = 0.0044$; *CHCHD2*^{T61I}-DMSO vs torin1, *ns*, $p = 0.0573$; *CHCHD2*$^{-/-}$-DMSO vs torin1, *ns*, $p = 0.1454$; CHCHD2 WT-DMSO vs *CHCHD2*^{T61I}-DMSO, *$p = 0.0121$; WT-DMSO vs *CHCHD2*$^{-/-}$-DMSO, *$p = 0.0174$; *CHCHD2*^{T61I}-DMSO vs *CHCHD2*$^{-/-}$-DMSO, *ns*, $p = 0.3191$; *CHCHD2*^{T61I}-torin1 vs *CHCHD2*$^{-/-}$-torin1, *$p = 0.0266$. (D) Autophagy flux assay in isogenic hESCs lines carrying *CHCHD2*^{T61I} or *CHCHD2*$^{-/-}$ treated with DMSO, torin1 250 nM or bafA1 100 ng/ml for 5 h. Quantification of MAP1LC3-II normalize with ACTB in hESCs. $n = 3$. Two-way ANOVA, **$p = 0.0011$; ***$p = 0.005$. (E) Co-immunoprecipitation of CHCHD2 by endogenous ULK1 bound to ULK1 antibody in lysates from isogenic hESC carrying CHCHD2 WT or *CHCHD2*^{T61I} *, unspecific band. (F) Proteins levels in lysates from isogenic hESCs carrying CHCHD2 or *CHCHD2*^{T61I}. Student t test, **$p = 0.0049$, $n = 3$.

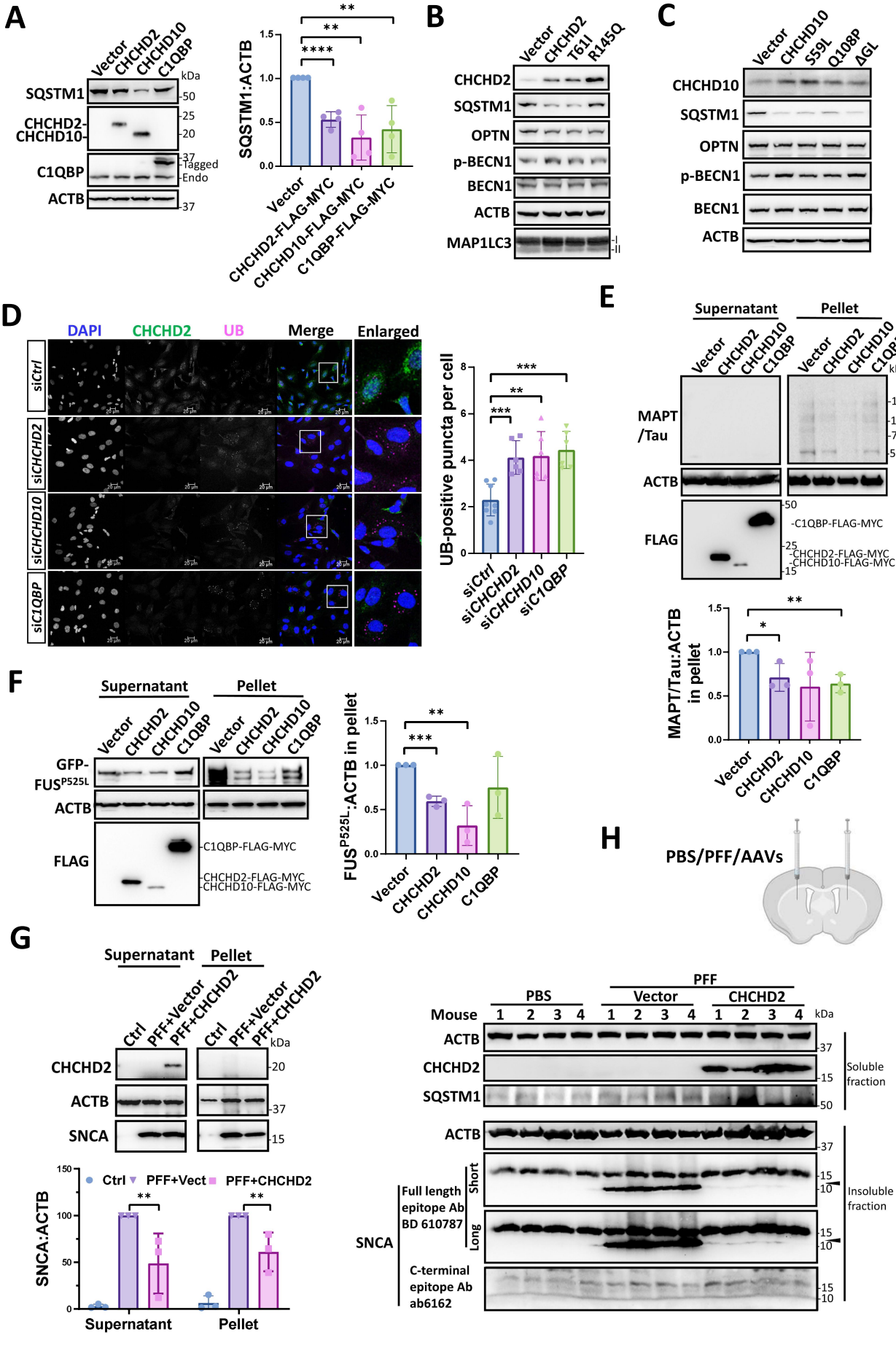

Figure 8. CHCHD2 promoted clearance of protein aggregates. (A-C) Western blot analysis on SK-N-SH cells transfected with control vector, C-terminal-tagged CHCHD2, CHCHD10 or C1QBP (A) with quantification, control vector, non-tagged CHCHD2 WT, CHCHD2^{T61I} or CHCHD2^{R145Q} (B), control vector, non-tagged CHCHD10

was detected in the insoluble fraction, as well as C-terminal truncation of SNCA evidenced by epitope-specific antibody (Figure 8(H)). C-terminal truncation of SNCA, was clearly reduced in the insoluble fraction from mouse striatum with expression of CHCHD2 (Figure 8H). A slight reduction of SQSTM1 was detected in CHCHD2-overexpressed brain lysates, suggesting autophagy activation. As C-terminal truncation of SNCA was highly toxic to accelerate formation of SNCA aggregates [86–90], the negative correlation between overexpressed CHCHD2 and reduced toxic C-terminal truncated SNCA suggested CHCHD2 helped to clear toxic SNCA species, therefore reducing protein aggregates. Collectively, CHCHD2 reduced protein aggregates in vitro and in vivo.

Discussion

Mutations in mitochondrial protein CHCHD2 or CHCHD10 causes neurodegeneration. Here we reported CHCHD2-CHCHD10-C1QBP complexed with ATG8s to promote autophagy and clear aggregates, revealing unexplored roles of CHCHD2 and CHCHD10 in proteostasis and providing novel insights in targeted therapy for neurodegeneration with aggregates (Figure 9).

CHCHD2-CHCHD10-C1QBP-ATG8 protein complex

We reported a protein complex composing of CHCHD2-CHCHD10-C1QBP-ATG8s. The identification of ATG8s as CHCHD2, CHCHD10 and C1QBP interactors provided biochemical foundation to unravel the hidden roles of CHCHD2, CHCHD10 and C1QBP in autophagy-lysosome pathway. Firstly, we examined how CHCHD2-CHCHD10-C1QBP complex assembled. We proved that C1QBP served as a scaffold for CHCHD2 and CHCHD10 interaction. N-terminal α-helix region of CHCHD2 and CHCHD10 strongly bound to C1QBP. CHCHD2 or CHCHD10 dimer formation was much weaker than CHCHD2-C1QBP or CHCHD10-C1QBP interaction. Besides, the N-terminal CHCHD2 was important for CHCHD2 homodimer formation. The C-terminal CHCHD2 mediated CHCHD2-CHCHD10 heterodimer formation, while the C-terminal CHCHD10 mediated CHCHD10 homodimer formation. Secondly, ATG8s bound to CHCHD2, CHCHD10 and C1QBP individually. In particular, ATG8s bound to both N and C termini of CHCHD2 and CHCHD10. ATG8s also helped CHCHD2-CHCHD10, CHCHD2-C1QBP and CHCHD10-C1QBP interaction to assemble a large protein complex. Within 2 LIRs in C1QBP, the 2nd LIR contributed more for C1QBP-ATG8 and C1QBP-CHCHD10 interaction. Taken together, CHCHD10 and CHCHD2, via their N-terminal α-helix, bound to C1QBP on the edge of prism of C1QBP trimer. ATG8s when binding to the 2nd LIR of C1QBP, was embedded in CHCHD2-CHCHD10-C1QBP complex. Meanwhile, the C terminus of CHCHD2 and CHCHD10, forming homo- and heterodimer, bound to another ATG8s (Figure 4J) and recruited ATG8-binding proteins such as ULK1 (Figures 6, 9). Considering the fast turnover of CHCHD2 and CHCHD10, the presence of CHCHD2-CHCHD10-C1QBP-ATG8s complex could be quite dynamic. Further crystallography or cryogenic electron microscopy studies may give ultimate answers.

In this complex, any single molecule simultaneously bound to a few others. Such multivalent architecture allows precise fit and increases the specificity and/or strength of protein-protein interaction. We speculate intricate organization of CHCHD2-CHCHD10-C1QBP-ATG8 complex safeguards its function. Mild errors in one component change some protein-protein interaction but do not disrupt the complex. Hence, the function of the complex could be largely maintained. Indeed, most disease-associated mutants of CHCHD2 or CHCHD10 still bound to other components, assembled the complex and functioned roughly well as their WT proteins (Figures 4, 8). However, chronic mild defects, possibly along with some uncorrectable environmental stress paradigm eventually break the balance and cause unfixable outcomes (Figure 9, S8). That could explain why CHCHD2 or CHCHD10 mutations-caused disorders are mostly late-onset and degenerative phenotypes in animal models are age-dependent.

Cytosolic CHCHD2 and CHCHD10

Autophagy is a cytoplasmic process, while CHCHD2 and CHCHD10 are mitochondrial proteins. Some CHCHD2 and CHCHD10 were present in the cytosol, but much less than in mitochondria. We showed both N and C termini of CHCHD2 and CHCHD10 contributed to their mitochondrial localization. Blocking either end, or mutation in N or C terminus, especially point mutations in CHCH domain (CHCHD2^{Q120P}, CHCHD10^{Q108P}) or N terminus (CHCHD2^{P14L} [11]), was strong enough to block mitochondrial localization. Mitochondrial C1QBP is also present in the cytosol [91]. Cell fractionation showed the presence of cytosolic

WT, CHCHD10^{S59L}, CHCHD10^{Q108P} or CHCHD10ΔGL (C) for 48 h. Unpaired t test, ****(vector vs CHCHD2), $p < 0.0001$; **(vector vs CHCHD10), $p = 0.0018$; **(vector vs C1QBP), $p = 0.0048$. (D) Confocal imaging of SK-N-SH cells transiently transfected with si*Control*, si*CHCHD2*, si*CHCHD10* or si*C1QBP* for 48 h. Cells were treated with 5 μg/ml puromycin for 2.5 h to induce aggregates. Endogenous CHCHD2 or Ubiquitin (UB) was labelled as green or violet. Scale bar: 20 μm. Right, quantification of UB positive puncta. 200-400 cells per group. Unpaired t test, ***$p = 0.0004$ (si*Ctrl* vs si*CHCHD2*); **$p = 0.0015$ (si*Ctrl* vs si*CHCHD10*); ***$p = 0.0002$ (si*Ctrl* vs si*C1QBP*). (E) Western blot analysis of soluble and insoluble fraction of HeLa cells transfected with control vector or CHCHD2-FLAG-MYC, CHCHD10-FLAG-MYC or C1QBP-FLAG-MYC with MAPT/Tau aggregates for 48 h. Quantification of MAPT/Tau:ACTB in the pellet. Unpaired t test, vector vs CHCHD2, *$p = 0.0337$; vector vs C1QBP, **$p = 0.0038$. (F) Western blot analysis of soluble and insoluble fraction of HeLa cells transfected with control vector, CHCHD2-FLAG-MYC, CHCHD10-FLAG-MYC or C1QBP-FLAG-MYC with aggregation-prone GFP-FUS^{P525L} for 48 h. Quantification of GFP-FUS^{P525L}:ACTB in the pellet. Unpaired t test, vector vs CHCHD2, ***$p = 0.0003$; vector vs CHCHD10, **$p = 0.0062$. (G) Western blot analysis of soluble and insoluble fraction of HeLa cells transfected with control vector or CHCHD2-FLAG-MYC with PFF 0.1 μg/ml for 48 h. Quantification of SNCA/α-synuclein: ACTB. 2-way ANOVA, **$p = 0.0035$ (PFF+Vect vs PFF+CHCHD2). (H) Illustration of intrastriatal PFF injection in the mouse brain. Immunoblot of SDS soluble and SDS insoluble fraction from the mouse striatum at 4-week post PFF and/or AAV injection. 4 out of 5 mice per group were shown. Arrow, C-terminal truncated SNCA/α-synuclein.

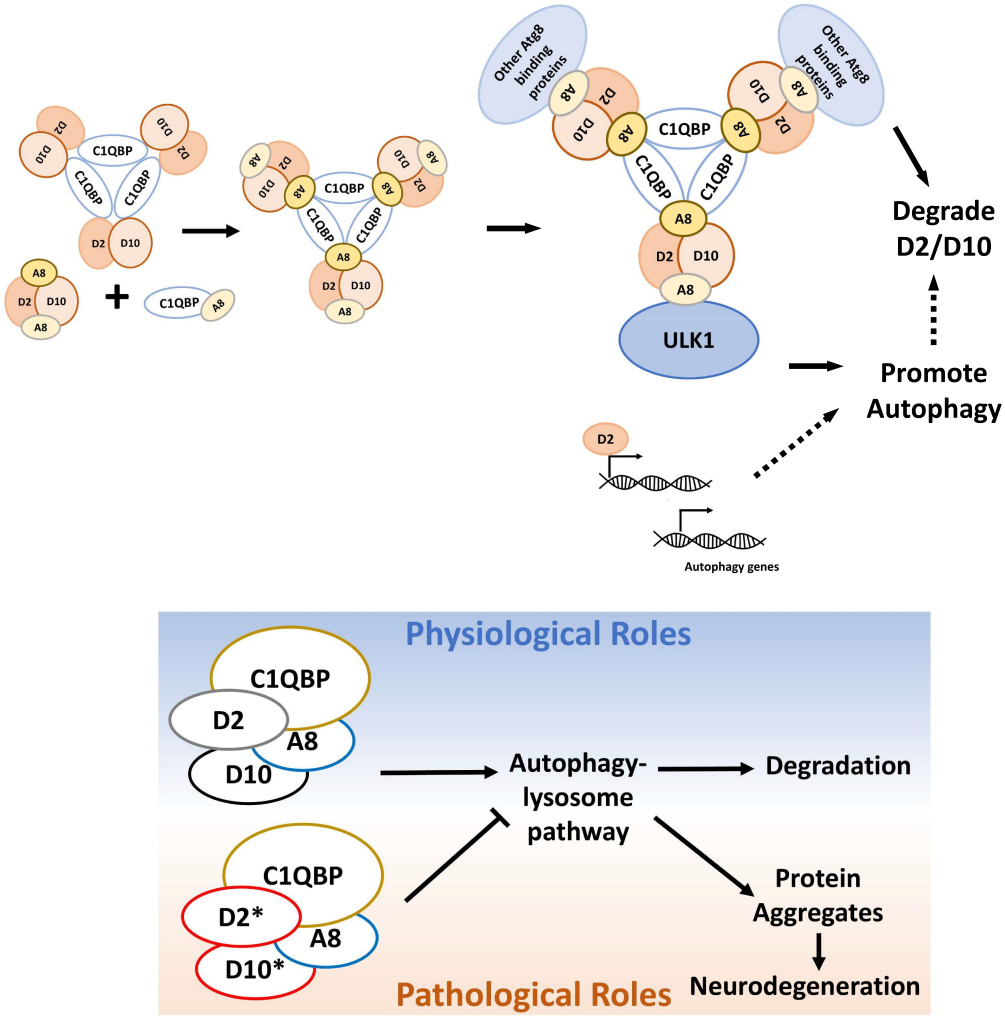

Figure 9. The schematic physiological roles of CHCHD2 and CHCHD10 in autophagy regulation and the pathogenic mechanisms of CHCHD2 and CHCHD10 mutants in neurodegeneration. CHCHD2, CHCHD10 and C1QBP, binding to ATG8s, formed a protein complex, in which C1QBP served as the scaffold to bring every component together. By binding to GABARAPs, CHCHD2 and CHCHD10 underwent autophagic degradation. CHCHD2, CHCHD10 and GABARAPs also recruited ULK1 complex to initiate autophagy. CHCHD2 may transcriptionally activate autophagy genes. Thus, autophagy was promoted. Disease-causing CHCHD2 or CHCHD10 mutations, such as CHCHD2^{T61I}, CHCHD10^{P34S} or CHCHD10^{S59L} showed altered interaction with ATG8s but did not disrupt the CHCHD2-CHCHD10-C1QBP-ATG8 complex and still carried out their roles in autophagy. However, chronic mild defects, possibly along with some environmental stresses, broke the balance, disturbed autophagy-lysosome pathway, eventually caused protein aggregates and neurodegeneration. Considering the high turnover of CHCHD2 and CHCHD10, such complex could be very dynamic and/or transient. D2, CHCHD2; D10, CHCHD10; A8, ATG8s; *,disease-associated mutations.

CHCHD2, CHCHD10 and C1QBP, supporting their roles in cytosolic autophagy. It is hard to capture a cytosol CHCHD2 and CHCHD10 by classical methods. The reasons could be: 1. Relatively low abundancy in cytosol while highly enriched in mitochondria; 2. Fast turnover of CHCHD2 and CHCHD10, especially when in cytosol. A cytosolic CHCHD10^{Q108P}, degraded ~5 fold faster than CHCHD10 WT [62].

Fast turnover of CHCHD2 and CHCHD10

Autophagy degrades long-lived cytosolic proteins and organelles [92]. Under normal conditions, most short-lived proteins are not primary targets for autophagy. However, by degrading specific short-lived proteins with regulatory functions in proteostasis, autophagy provides a mechanism for rapid stimulus responsiveness and prompt, demand-driven regulation. The turnover rate of CHCHD2 and CHCHD10 is too fast for typical autophagy substrates when proteins with $t_{1/2}$ < 8 h are regarded as short-lived proteins [93]. Here we showed that CHCHD2 and CHCHD10 were autophagic substrates and autophagy activators, in that CHCHD2 and CHCHD10 promoted autophagy while such activated autophagy may degrade themselves. Fast turnover of CHCHD2 and CHCHD10 could be due to sophisticated regulatory mechanisms on them. Firstly, CHCHD2 functions as a transcription factor of itself [94,95]. There could be a positive feedback loop of CHCHD2's self-amplification where CHCHD2 promoted the transcription of itself, thus producing more CHCHD2 protein. Secondly, there could be a negative feedback loop of CHCHD2 post-translationally, where CHCHD2 functioned as both an autophagy substrate

and activator, allowing the system to speed up autophagy machinery to clear some autophagic substrates, possibly along with CHCHD2 and CHCHD10, hence offset against CHCHD2's self-amplification. Interestingly, CHCHD2 or CHCHD10 mutations which lost or reduced their C-terminal ATG8 binding had longer half-life than WT proteins but still underwent degradation, suggesting more degradation mechanisms of CHCHD2 and CHCHD10. As our study showed CHCHD2 was not degraded by UB-dependent proteosome degradation pathway, nuclear CHCHD2 could be degraded by a UB-independent proteosome pathway via MIDN (midnolin) [96], whose structure variant was regarded as a genetic risk for PD [97,98]. Further studies are needed.

CHCHD2 in autophagy regulation

We reported CHCHD2 and CHCHD10 promoted autophagy. CHCHD2 was firstly identified as a bi-organelle protein in nuclear and mitochondria. When in nuclear, CHCHD2 functions as a transcription factor to regulate some mitochondrial proteins, mtUPR and itself [99,100]. A CHIP-seq analysis of adenovirus-transfected CHCHD2 on primary mouse hepatocytes showed that 90% of 3769 CHCHD2 peaks were located in the promoter regions of genes [95]. We retrieved this data, and found top CHCHD2 target genes on enriched Kyoto Encyclopaedia of Genes and Genomes (KEGG) pathways were protein processing (1st), autophagy (2nd), ALS (6th), AMPK (AMP-activated protein kinase) pathway (19th), PD (24th), AD (30th) and HTT (Huntingtin) (44th) (Table S1). Among them, key autophagy regulators transcripts were seen, including *Map1lc3b*, *Gabarap*, *Gabarapl1*, *Ulk2*, *Atg13*, *Rab1a*, *Atg5*, *Atg9a*, *Atg9b*, *Wipi1*, *Wipi2*. Those results suggested CHCHD2 transcriptionally upregulates autophagic genes but such regulation may or may not be direct. We tested some hits in SK-N-SH cells upon transient *CHCHD2* knockdown, along with transient *CHCHD10* or *C1QBP* knockdown. si*CHCHD2* or si*CHCHD10* did not reduce the expression of autophagic genes, while si*C1QBP* significantly upregulated autophagic genes such as *ULK1*, *ULK2*, *UVRAG*, *ATG3* and *LC3B* (Figure S9O), suggesting the transcriptional roles of CHCHD2 could be achieved by its associating complex. Interestingly, *C1QBP* knockdown enhanced *CHCHD2* (Figure S9O), even with a reduction of CHCHD2 protein level (Figure S9M), hinting at a further regulatory loop between CHCHD2 and C1QBP. Taken together, CHCHD2's role on autophagy activation could be attributed to: a direct protein-protein interaction via CHCHD2-CHCHD10-C1QBP-GABARAPs complexed with ULK1, and a possible indirect transcriptional upregulation of autophagy genes by CHCHD2 and its associating proteins (Figure 9). Meanwhile, transient *CHCHD2* knockdown caused multiple cellular defects but chronic *CHCHD2* KO showed mild or even no phenotypes. We previously proposed the presence of compensatory effects from its paralog CHCHD10 [14], which was later proven as partially [28,37]. Here we speculate the transcriptional roles of CHCHD2 [95,99], possibly with its binding partners, also contribute to the difference between transient and chronic manipulation with transcriptional adaptation during long-term genetic engineering [101].

We reported the physiological roles of CHCHD2 and CHCHD10 in autophagy initiation via GABARAPs-ULK1. ATG8s play roles in almost every step of autophagy-lysosome pathway. It is also possible CHCHD2 or CHCHD10 involves in other stages in autophagy-lysosome pathways. As current study excluded the possibility of CMA, further study may reveal whether they participate in additional related mechanisms, such as ESCRT (endosomal sorting complex required for transport) machinery.

CHCHD2 and CHCHD10 functioned as not only autophagy substrates but also promoted autophagy. Those two aspects of CHCHD2 and CHCHD10 may be closely interrelated. Actually, some autophagy regulators themselves are substrates for autophagy, showing a complex feedback loop where the machinery regulates itself to maintain balance. It is likely CHCHD2 and CHCHD10 degraded along with the autophagy activated by itself. Similar situation was seen in CCT2 (chaperonin containing TCP1 subunit 2) [102]. CCT2 functions as an autophagy receptor that specifically targets and facilitates the degradation of solid protein aggregates. It is also a substrate of the aggrephagy pathway itself and degraded along with the cargo it delivers. These tightly coordinated biological processes enable cells to respond rapidly and accurately to both internal and external signals to sustain cellular health and functionality.

CHCHD2 and CHCHD10 in protein aggregates clearance

Many neurodegenerative disease-related aggregates were cleared by autophagy [103–107]. Many CHCHD2 or CHCHD10 mutants caused protein aggregates in vivo. Interestingly, CHCHD10 reduces TARDBP aggregates in cell and mouse model [34]. Our study mechanistically revealed a direct role of CHCHD2 and CHCHD10 in autophagy, specifically in aggregate clearance. CHCHD2 reduced aggregated SNCA initiated by PFF, suggesting CHCHD2 cleared aggregates, a function similar to CCT2 [102]. CCT2 promotes clearance of solid protein aggregates [102]. CHCHD2 was co-captured with CCT2 by mass spectrometry when searching for proteins binding HTT aggregates in U2OS cells, though less enriched than CCT2 [102]. CHCHD2 or CHCHD10 mutations caused protein aggregates including SNCA, TARDBP, CHCHD2 and/or CHCHD10 *etc.*, suggesting CHCHD2 and CHCHD10 associated with protein aggregates in a generalized manner. This could be mediated by physical interaction via liquid-liquid phase transition (LLPS) of biocondensates or protein aggregates [108,109]. ATG8s, the newly identified CHCHD2 and CHCHD10 interactors, are actively involved in LLPS. Moreover, GABARAPs were specifically associated with SNCA oligomer but not SNCA monomer [110]. GABARAPs were also functionally related to protein aggregates. Loss of GABARAPs contributed more to protein aggregates formation than loss of MAP1LC3s [84]. With more studies on the specificity of GABARAP subfamily vs MAP1LC3 subfamily [111,112], our study on CHCHD2 and CHCHD10's association with GABARAPs to clear

protein aggregates corroborated those findings to highlight the significance of less-studied GABARAPs in protein aggregate clearance. Further long-term investigations using CHCHD2 overexpression in PFF mouse model could reveal functional connections and offer holistic insights into the impact of CHCHD2 on the processing and clearance of protein aggregates.

C1QBP in autophagy and mitophagy

C1QBP plays pleiotropic cellular roles with numerous interactors [113]. We reported C1QBP associated with ATG8s directly. Considering the high abundancy of C1QBP and ATG8s, with strong binding affinity between C1QBP-ATG8s, a C1QBP-ATG8s interaction could be one missing fundamental mechanism of its pleiotropic cellular roles. Notably, cardiomyocyte-specific *c1qbp*$^{-/-}$ in mice showed autophagy defects [59]. C1QBP was reported to bind to ULK1 directly [114]; our data instead suggested C1QBP interacted with ULK1 via ATG8s, CHCHD10 and CHCHD2. We confirmed 2 LIRs in C1QBP for ATG8s and CHCHD10 interaction, providing mechanistic insights of C1QBP function in autophagy. Of note, compound heterozygous mutations including 1st LIR of C1QBP associated with fatal human cases [54], suggesting C1QBP-ATG8 interaction is pivotal in vivo. 1st LIR of C1QBP is at flexible region above or below the prism of C1QBP trimer showed by crystal structure, and 2nd LIR of C1QBP is at the edge of prism, mediating CHCHD2 and CHCHD10 interaction. Further studies on 1st LIR of C1QBP are needed. Alternatively, ULK1-ATG8s was recruited to mitochondria by interacting with mitochondrial FUNDC1 (FUN14 domain containing 1) [115]. We envision that mitochondrial CHCHD2, CHCHD10 and C1QBP could recruit ULK1 and ATG8s to promote PINK1-PRKN/Parkin-independent mitophagy. The findings of this study have to be seen in light of some limitations. Due to the nature of fast decay of CHCHD2 and CHCHD10 and multiple ATG8 isoforms with their functional redundancy and compensation, many results here had to be based on relative short-term overexpression or in vitro studies. Further studies on endogenous protein tagging may help to decipher fine regulation of this protein complex in versatile cellular mechanisms.

Mutations of mitochondrial proteins CHCHD2 or CHCHD10 caused neurodegeneration with protein aggregates. Our study suggested chronic disrupted proteostasis underlay CHCHD2 or CHCHD10 mutations-associated neurodegeneration. We reported CHCHD2 and CHCHD10 as both autophagy substrates and autophagy receptors to clear protein aggregates. With low CHCHD2 in PD patients [116] and low CHCHD10 in ALS or FTD patients [117], restoring CHCHD2 or CHCHD10 hold the potential to rejuvenate autophagy and mitochondria to benefit patients.

Materials and methods

Animals

Mouse husbandry and procedures were performed in accordance with the guidelines of Laboratory Animal Manual of the National Institute of Health Guide to the Care and Use of Animals and upon approval of DUKE-NUS Graduate Medical School Institute Animal Care and Use Committee (2020/SHS/1549). Male C57BL/6 mice (The Jackson Laboratory, 000664) were used.

Cell culture

SK-N-SH cells (ATCC, HTB-11) were maintained in Minimal Essential Medium Eagle (Sigma) supplemented with 10% FBS (Hyclone, SH30071.03E) with NEAA (Non-Essential Amino acids) (Gibco, 11140050). HeLa cells (ATCC, CRM-CCL-2) were maintained in DMEM (Gibco, 11965092) supplemented with 10% FBS. siRNA or plasmid transfection was mediated by TurboFect^{TM} (Thermo Fisher Scientific Inc., R0531).

Dopaminergic neuron differentiation and characterization

To establish H9-*TH*-EGFP cell line, the fluorescent reporter EGFP were directly inserted before the *TH* stop codon using the CRISPR/Cas9 system. with sgRNA (5'-AGTGCCATTGGCTAGGTGCACGG −3') targeting exon 14 of *TH* gene right before the stop codon, together with a plasmid donor carrying homology-directed repair (HDR) template with T2A-EGFP sequence. *CHCHD2*$^{-/-}$ was generated using sgRNA (5'-TCCGGCCAGGTGAGACCATC-3') targeting exon 1 of the *CHCHD2* gene. *CHCHD2*^{T61I} was generated using sgRNA (5'-CACCGTTGGGTCACGCCATTACTGG-3') targeting exon 2 of the *CHCHD2* gene, together with a plasmid donor carrying HDR template with *CHCHD2 Thr61Ile* mutation. Cells were selected by puromycin for 2 days before being plated as single cells for colony picking. Clones were selected by PCR amplification for targets of interest. All selected clones were screened for potential off-target sites. Karyotyping was done by Cytogenetics Lab in Singapore General Hospital (Singapore).

Midbrain-like organoids were generated as previously described with some modifications [118]. Briefly, 70–80% confluent hESC was dissociated into single cells by TrypLE^{TM} Express Enzyme (Thermo Fisher Scientific Inc., 12605010) and seeded into 96-well U bottom Ultra-Low Attachment plate with a density of 4000 to 6000 cells per well and supplemented with 10 μM ROCK inhibitor Y27632 (Calbiochem, 331752-47–7). From day 2 to day 6, the following midbrain patterning factors were added: 10 μM SB431542, 100 nM LDN193189, 0.75 μM purmorphamine, 0.7 μM CHIR99021. From day 4 to day 12, 100 ng/ml FGF8 was added. At day 6, each organoid was embedded in 20 μl of Growth Factors Reduced Matrigel (Corning, 354230) and transferred to 6-well plates on an orbital shaker with 70 rpm at day 8. After initial 12 days of patterning, organoids were maintained in organoid media consisting of Neurobasal (Gibco, 21103049) supplemented with NeuroCult^{TM} SM1 Neuronal Supplement (STEMCELL Technologies, 06711), 1 M HEPES, 1 × Antibiotic-Antimycotic (Gibco, 15240062), and 1 × Glutamax^{TM} (Gibco, 35050061). Neurotrophic factors of 100 μg/ml BDNF (STEMCELL Technologies, 78005.1) and 100 μg/ml GDNF (STEMCELL Technologies, 78005.1), and 200 mM c-dbAMP (Sigma-Aldrich Co. LLC, D0627)

were added as needed. Midbrain-like organoids were dissociated using papain (Worthington Biochemical Corporation, 9001-73-4) at day 50. Dissociated cells were plated on either Matrigel-coated or poly-l-lysine (PLL) or laminin-coated glass coverslips at a density of 70,000 to 100,000 cells per coverslip. Cells were given 2 to 3 days to attach onto the coverslips, for further drug treatment and immunofluorescence assay.

Plasmid constructs, mutagenesis and RNAi interference

Point mutations of *CHCHD2, CHCHD10 or C1QBP* were introduced into the coding sequence of respective cDNA with Site-directed mutagenesis kit (Stratagene, 200518). For bacterial expression of GST-tagged CHCHD2, CHCHD10, or C1QBP plasmids, pGEX-5X-1 vectors (GE Healthcare, 28–9545-53) were digested with Sal I and Not I (New England Biolabs, R0138S and R0189S) and ligated with the following fragments: *CHCHD2* gene, PCR amplified from the pCMV6-CHCHD2 vector; *CHCHD10* gene, PCR amplified from the pCMV6-CHCHD10 vector; *C1QBP* gene, PCR amplified from the pCMV6-C1QBP vector. For bacterial expression of His-tagged CHCHD2, CHCHD10, C1QBP, pET-15b vector were digested by BamH I and Xho I and ligated with respective fragments. N-terminal HA-FLAG-tagged CHCHD2 and CHCHD2^{Q126X} were cloned to pCDNA3-N-HA-FLAG vector from Addgene by using EcoR I and Xho I sites. All plasmids are listed in Table 1. All primers used for the cloning and mutagenesis are listed in Table 2. The detailed information of RNAi is listed in Table 3.

Recombinant protein expression and purification

Recombinant proteins of His- or GST-tagged CHCHD2, CHCHD10, or their mutations CHCHD2^{T61I}, CHCHD2^{R145Q}, CHCHD10^{P34S}, CHCHD10^{S59L} were expressed in SHuffle T7 Express Escherichia coli to promote disulfide bond formation. Recombinant proteins of C1QBP were expressed in BL21(DE3) Escherichia coli. Transformed bacteria were grown in LB Broth with Ampicillin at 28-30°C and induced with 0.2 mM isopropyl β-d-1-thiogalactopyranoside (IPTG, Sigma-Aldrich CO. LLC, I6758) for 3-4 h. Bacteria cells were harvested by centrifugation. For purification, bacteria were resuspended in buffer (50 mM Tris-HCl, pH 8.0, 500 mM NaCl, 10% glycerol, 2 mM EDTA, 1% Triton X-100 (Bio-Rad Laboratories, Inc., 161-0407), 5 mM imidazole for His proteins) supplemented with lysozyme (Thermo Fisher Scientific Inc., 90082). Sonication was carried out for bacterial expressing recombinant CHCHD10 or C1QBP proteins. Soluble fraction of bacterial lysates was obtained after centrifugation. The soluble supernatant was incubated with equilibrated GST Agarose beads (Thermo Scientific Scientific Inc., 16100) or Ni-NTA beads (QIAGEN, N.V., 1018244) for 1-2 h at 4°C. After extensive washing of the beads with buffer, freshly prepared GST fusion protein bound-beads or His protein-bound beads were used in following analysis; otherwise, proteins were eluted from GST or His beads with elution buffer containing 15 mM glutathione or 250 mM imidazole. The eluted proteins were then concentrated by Amicon Ultra Centrifugal Filters (Millipore, UFC800324). Proteins were quantified, flash frozen and stored at -80°C.

GST affinity isolation, immunoprecipitation and in vitro binding assay

For GST affinity isolation, GST beads bound with freshly prepared recombinant GST-fused WT or mutant proteins were incubated with mammalian cell lysates for 2-3 h at 4°C, followed by extensive washing to remove unspecific binding proteins. The affinity-isolated complex was then dissolved in 2 × SDS-PAGE sample buffer and subjected to following analysis. For immunoprecipitation, mammalian cells were harvested with lysis buffer containing 50 mM Tris-HCl, pH 7.4, 150 mM NaCl, 1% Triton X-100 with EDTA and proteinase inhibitor (Thermo Fisher Scientific Inc., 78429). Lysates, which is the supernatant after centrifugation at 20,817 × *g* for 15 min at 4°C, were then pre-cleared with Protein A/G Sepharose beads (Thermo Fisher Scientific Inc., 20421). The flowthrough was incubated with either control IgG or specific antibodies at 4°C, followed with fresh Sepharose beads. Unspecific binding proteins were removed by extensive washing. The immunoprecipitated complex was then eluted by 0.2 M glycine pH 2.0 with 0.15 M NaCl and subject to immunoblotting. Input samples were collected prior to mixing with beads and 2-4% (for whole cell lysates) of the input samples were used for immunoblotting analysis. For in vitro protein binding analysis, purified GST-tagged proteins were immobilized on GST-agarose beads (or His-tagged proteins were immobilized on Ni-NTA agarose beads), mixed with purified 3-5 µg His-tagged proteins (or GST-tagged proteins) in 50 mM HEPES, pH 7.4, 150 mM NaCl and 0.25% NP-40 (Sigma-Aldrich CO. LLC, 74385) for 3 h at 4°C with agitation. Beads were washed to remove the unspecific binders. The beads with interacting proteins were dissolved in 2 × SDS-PAGE sample buffer and subjected to following analysis. All antibodies are listed in Table 4 and 5.

Proteomic analysis using LC-MS/MS (liquid chromatography-tandem mass spectrometry)

Briefly, in-gel digestion was performed. Resulting peptides were reconstituted in 2% Acetonitrile, 0.1% formic acid in water and peptide concentration was determined by Thermo Scientific™ Pierce™ Quantitative Fluorescent Peptide Assay. The reconstituted peptide samples were then analyzed on an EASY-nLC 1200 system coupled to Orbitrap Exploris™ 480 mass spectrometer (Thermo Fisher Scientific Inc., BRE725539). The Easy-nLC system was equipped with an in-line trap column of PepMap 100 C18, 3 µm, 75 µm × 2 cm (Thermo Fisher Scientific Inc., 164943) and Easy-spray Pepmap RSLC C18, 2 µm, 15 cm × 75 µm column. The EASY-nLC was operated at a flow rate of 300 nL/min. Mobile phase A consisted of 0.1% formic acid in LC-MS grade water and mobile phase B was made up of 0.1% formic acid, 80% acetonitrile in LC-MS grade water. A step gradient was utilized from 5% to 60% mobile phase B for 29 min, followed by 1 min from 60% to 98% solvent B. Some important settings for Orbitrap 480 MS are as follows: data was acquired using data-dependent acquisition (DDA) in positive mode; resolution for MS1 and MS2 scans: 60,000 and 15,000; MS1

Table 1. Plasmids.

Plasmids	Resource	Identifier
CHCHD2-non-tagged	Origene^{TM} Technologies	sc114478
CHCHD10-non-tagged	Origene^{TM} Technologies	sc308703
CHCHD2-FLAG-MYC	Origene^{TM} Technologies	RC209806
CHCHD10-FLAG-MYC	Origene^{TM} Technologies	RC209077
CHCHD4-FLAG-MYC	Origene^{TM} Technologies	RC217831
MYC-LAMP2A	Origene^{TM} Technologies	RC221216
N-HA-FLAG-pcDNA3	Addgene	10792 (William Sellers Lab)
C1QBP-FLAG-MYC	Origene^{TM} Technologies	RC201742
pGEX-5x-1	Sigma-Aldrich Co. LLC	28-9545-53
pET-15b	Novagen- Merck & Co., Inc	69661
pSNAPf vector	New England Biolabs, Inc	N9183S
pSNAPf-COX8A	Addgene	101129 (Ana Egana Lab: Egana Lab NEB plasmids)
PARK7/DJ-1-pSNAPf	This paper	N/A
mCherry-ZFYVE1	Addgene	86746 (Do-Hyung Kim Lab)
pEGFP-C1-LC3A	This paper	N/A
pEGFP-C1-LC3B	This paper	N/A
FLAG-LC3C	Addgene	123095 (Robin Ketteler Lab)
pEGFP-C1-GABARAP	Addgene	87871 (Eiki Kominami Lab)
pEGFP-C1-GABARAPL1	This paper	N/A
pEGFP-C1-GABARAPL2	This paper	N/A
HA-ULK1	Addgene	31963 (Do-Hyung Kim Lab)
GST-LC3A	Addgene	73946 (Dieter Willbold Lab)
GST-LC3B	This paper	N/A
GST-LC3C	This paper	N/A
GST-GABARAP	Addgene	73948 (Dieter Willbold Lab)
GST-GABARAPL1	Addgene	73945 (Dieter Willbold Lab)
GST-GABARAPL2	Addgene	73518 (Dieter Willbold Lab)
His-LC3A	This paper	N/A
His-LC3B	Addgene	73949 (Dieter Willbold Lab)
His-LC3C	This paper	N/A
His-GABARAP	This paper	N/A
His-GABARAPL1	This paper	N/A
His-GABARAPL2	This paper	N/A
Non-tagged CHCHD2^{T61I}	[14]	N/A
Non-tagged CHCHD2^{Q126X}	[14]	N/A
Non-tagged CHCHD2^{R145Q}	[14]	N/A
CHCHD2^{T61I}-FLAG-MYC	This paper	N/A
CHCHD2^{R145Q}-FLAG-MYC	This paper	N/A
CHCHD2^{Q120P}-FLAG-MYC	This paper	N/A
N-HA-FLAG-CHCHD2	This paper	N/A
N-HA-FLAG-CHCHD2 ^{Q126X}	This paper	N/A
pGEX-5x-1-CHCHD2	This paper	N/A
pGEX-5x-1-CHCHD2^{T61I}	This paper	N/A
pGEX-5x-1-CHCHD2^{R145Q}	This paper	N/A
pGEX-5x-1-CHCHD2^{Q126X}	This paper	N/A
pGEX-5x-1-CHCHD2^{R145X}	This paper	N/A
pGEX-5x-1-CHCHD2^{R149X}	This paper	N/A
pGEX-5x-1-CHCHD2-N (1-89)	This paper	N/A
pGEX-5x-1-CHCHD2-C (90-151)	This paper	N/A
pET-15b-CHCHD2	This paper	N/A
CHCHD2-pSNAPf	This paper	N/A
pSNAPf-CHCHD2	This paper	N/A
Non-tagged CHCHD10^{P34S}	This paper	N/A
Non-tagged CHCHD10^{S59L}	This paper	N/A
Non-tagged CHCHD10^{Q108P}	This paper	N/A
Non-tagged CHCHD10ΔGL145146	This paper	N/A
CHCHD10^{S59L}-FLAG-MYC	This paper	N/A
CHCHD10^{Q108P}-FLAG-MYC	This paper	N/A
CHCHD10ΔGL145146-FLAG-MYC	This paper	N/A
N-HA-FLAG-CHCHD10	This paper	N/A
N-HA-FLAG^{Q108X} -CHCHD10	This paper	N/A
pGEX-5x-1-CHCHD10	This paper	N/A
pGEX-5x-1-CHCHD10^{Q108X}	This paper	N/A
pGEX-5x-1-CHCHD10^{Q131X}	This paper	N/A
pGEX-5x-1-CHCHD10^{Y134X}	This paper	N/A
pGEX-5x-1-CHCHD10ΔGL145146	This paper	N/A
pGEX-5x-1-CHCHD10-N (1-82)	This paper	N/A
pGEX-5x-1-CHCHD10-C (83-142)	This paper	N/A
pET-15b-CHCHD10	This paper	N/A
CHCHD10-pSNAPf	This paper	N/A
CHCHD10^{Q108P}-pSNAPf	This paper	N/A
pSNAPf-CHCHD10	This paper	N/A
C1QBP^{4243AA}-FLAG-MYC (D1)	This paper	N/A
C1QBP^{236237AA}-FLAG-MYC (D2)	This paper	N/A
C1QBP^{4243AA236237AA}-FLAG-MYC (DD)	This paper	N/A
pGEX-5x-1-C1QBP	This paper	N/A
pGEX-5x-1-C1QBP^{4243AA} (D1)	This paper	N/A
pGEX-5x-1-C1QBP^{236237AA} (D2)	This paper	N/A

(*Continued*)

Table 1. (Continued).

Plasmids	Resource	Identifier
pGEX-5x-1-C1QBP^{4243AA236237AA} (DD)	This paper	N/A
pET-15b-C1QBP	This paper	N/A
pET-15b-C1QBP^{4243AA} (D1)	This paper	N/A
pET-15b-C1QBP^{236237AA} (D2)	This paper	N/A
pET-15b-C1QBP^{4243AA236237AA} (DD)	This paper	N/A
pAH-LAP-HA-P525L-FUS	[119]	N/A (Ling Shuo-Chien Lab)
GFP-LC3-RFP-LC3ΔG	[82]	84572 (Noboru Mizushima Lab)

Table 2. Primers for cloning or mutagenesis.

Name	Sequence 5′->3′
CHCHD2^{T61I}-F	CCCAGATGGCAATCACTGCAGCTGG
CHCHD2^{T61I}-R	CCAGCTGCAGTGATTGCCATCTGGG
CHCHD2^{Q120P}-F	CTCTATGAGATCAAACCCTTTCTGGAGTGTGCCC
CHCHD2^{Q120P}-R	GGGCACACTCCAGAAAGGGTTTGATCTCATAGAG
CHCHD2^{R145X}-F	GGTGCTGAAACAGTGCTGACTTGCAAACGGATTG
CHCHD2^{R145X}-R	CAATCCGTTTGCAAGTCAGCACTGTTTCAGCACC
CHCHD2^{G149X}-F	GTGCCGACTTGCAAACTGATTGGCCTAATGAAG
CHCHD2^{G149X}-R	CTTCATTAGGCCAATCAGTTTGCAAGTCGGCAC
CHCHD10^{P34S}-F	GGCAGCCGCCTCAGCCCCCGC [40]
CHCHD10^{P34S}-R	GCGGGGGCTGAGGCGGCTGCC [40]
CHCHD10^{S59L}-1-F	GTAGCCGTGGGCTTGGCTGTGGGACAC
CHCHD10^{S59L}-1-R	GTGTCCCACAGCCAAGCCCACGGCTAC
CHCHD10^{Q108X}-F	CCTACGAGATCAGGTAGTTCCTGGACTG
CHCHD10^{Q108X}-R	CAGTCCAGGAACTACCTGATCTCGTAGG
CHCHD10^{Q131X}-F	CGAGGCCCTGAAGTAGTGCAAGTACTAC
CHCHD10^{Q131X}-R	GTAGTACTTGCACTACTTCAGGGCCTCG
CHCHD10^{Y134X}-F	GAAGCAGTGCAAGTAGTACCATGGTCTGAG
CHCHD10^{Y134X}-R	CTCAGACCATGGTACTACTTGCACTGCTTC
CHCHD10^{Q108P}-F	CTACGAGATCAGGCCCTTCCTGGACTGTTC
CHCHD10^{Q108P}-R	GAACAGTCCAGGAAGGGCCTGATCTCGTAG
CHCHD10ΔGL-F	CAAGTACTACCATAGCTCCCTGCCC
CHCHD10ΔGL-R	GGGCAGGGAGCTATGGTAGTACTTG
C1QBP^{4344AA}-F	CTGTGCACCCGGCCCGCCGCCCTGCTCAGCGTGCG
C1QBP^{4344AA}-R	CGCACGCTGAGCAGGGCGGCGGGCCGGGTGCACAG
C1QBP^{236237AA}-F	CCTTGGACTGGGCCTTAGCCGCCCACCTAATGGATTTCC
C1QBP^{236237AA}-R	GGAAATCCATTAGGTGGGCGGCTAAGGCCCAGTCCAAGG
CHCHD2-SNAP-NheI-F	GCTAGCGCTAGCGCCACCATGCCGCGTGGAAGCCGAAG
CHCHD2-SNAP-AgeI-R	ACCGGTACCGGTGGCCAATCCGTTTGCAAGTCG
CHCHD10-SNAP-NheI-F	GCTAGCGCTAGCTCGCCACCATGATGCCTCGGGGAAGCCGCA
CHCHD10-SNAP-AgeI-R	ACCGGTACCGGTGGGCAGGGAGCTCAGACCATG
PARK7/DJ-1-SNAP-NheI-F	GCTAGCGCTAGCGCCACCATGATGGCTTCCAAAAGAG
PARK7/DJ-1-SNAP-AgeI-R	ACCGGTACCGGTGTCTTTAAGAACAAGTGGAGCCTTC
SNAP-CHCHD2-BamHI-F	GGATCCGGATCC ATG CCGCGTGGAAGCCGAAGC
SNAP-CHCHD2-NotI-R	GCGGCCGCGCGGCCGCTTAGGCCAATCCGTTTGCAAG
SNAP-CHCHD10-BamHI-F	GGATCCGGATCC ATG CCTCGGGGAAGCCGCAG
SNAP-CHCHD10-NotI-R	GCGGCCGCGCGGCCGCTCAGGGCAGGGAGCTCAGACC
N-SalI-CHCHD2-pGEX-5x-F	GTCGACGTCGACTCATGCCGCGTGGAAGCCGAAG
C-NotI-CHCHD2-pGEX-5x-R	GCGGCCGCGCGGCCGCGAACTTCTTCATTAGGCCAATCC
N-SalI-CHCHD10-pGEX-5x-F	GTCGACGTCGACTCATGCCTCGGGGAAGCCGCAG
C-NotI-CHCHD10-pGEX-5x-R	GCGGCCGCGCGGCCGCTCAGGGCAGGGAGCTCAGACCATG
N-BamHI-C1QBP-pGEX-5x-F	GGATCCGGATCCCCATGCTGCCTCTGATG
C-XhoI-C1QBP-pGEX-5x-R	CTCGAGCTCGAGCTACTGGCTCTTGACAAAAC
N-NdeI-CHCHD2-PET15b-F	CATATGCATATGATGCCGCGTGGAAGC
C-BamHI-CHCHD2-pET15b-R	GGATCCGGATCCTTAGGCCAATCCG
N-NdeI-CHCHD10-pET15b-F	CATATGCATATGATGCCTCGGGGAAGCCGCAG
C-BamHI-CHCHD10-pET15b-R	GGATCCGGATCCTCAGGGCAGGGAGCTCAGAC
N-NdeI-C1QBP-pET15b-F	CATATGCATATGATGCTGCCTCTGCTGCGCTG
C-BamHI-C1QBP-pET15b-R	GGATCCGGATCCTTACTGGCTCTTGACAAAAC
N-SalI-CHCHD2$^{1-89}$-F	GTCGACGTCGACTCATGCCGCGTGGAAGCCGAAG
C-NotI-CHCHD2$^{1-89}$-R	GCGGCCGCGCGGCCGCGAAATTACTTCCTCCACTGAAG
N-SalI-CHCHD2$^{90-151}$-F	GTCGACGTCGACTCGCTGAGCCTGCGAGGCCTGAC
C-NotI-CHCHD2$^{90-151}$-R	GCGGCCGCGCGGCCGCGAACTTCTTCATTAGGCCAATCC
N-SalI-CHCHD10$^{1-82}$-F	GTCGACGTCGACTCATGCCTCGGGGAAGCCGCAG
C-NotI-CHCHD10$^{1-82}$-R	GCGGCCGCGCGGCCGCTTACTGGGAGGGCTCCGAGCTG
N-SalI-CHCHD10$^{83-142}$-F	GTCGACGTCGACTCCCTGCTGTCCAGCAGGCCCCCACC
C-NotI-CHCHD10$^{83-142}$-R	GCGGCCGCGCGGCCGCTCAGGGCAGGGAGCTCAGACCATG

Table 3. siRNAs.

Gene	siRNA sequence	Cat No	Resource
CHCHD2		L-019120-01-0005 (OnTarget Plus, SMARTPool)	Dharmacon™, Thermo Fisher Scientific Inc.
		LQ-019120-01-0002 (OnTarget Plus, set of 4)	Dharmacon™, Thermo Fisher Scientific Inc.
CHCHD10		L-032555-01-0005 (OnTarget Plus, SMARTPool)	Dharmacon™, Thermo Fisher Scientific Inc.
C1QBP		L-011225-01-0005 (OnTarget Plus, SMARTPool)	Dharmacon™, Thermo Fisher Scientific Inc.
LAMP2A	GCACCAUCAUGCUGGAUAUUU, GUGCAGAUGACGACAACUUUU, UUCUAGUGUUGCUGGCUUAUU	customized LAMP2A of exon 9a, CTM-760878, 80, 81	Dharmacon™, Thermo Fisher Scientific Inc.
LONP1		sc-97290	Santa Cruz Biotechnology
AFG3L2		sc-72464	Santa Cruz Biotechnology
YME1L1		sc-90696	Santa Cruz Biotechnology
CLPP		sc-60413	Santa Cruz Biotechnology
HTRA2		sc-35615	Santa Cruz Biotechnology
ATG5		S18158, Silencer® selected	Thermo Fisher Scientific Inc.
ATG7		S20650, Silencer® selected	Thermo Fisher Scientific Inc.

and MS2 AGC target: 300% and 75%; MS2 isolation window: 1.6 Th; MS2 HCD Collision Energy: 28%. The resulting MS/MS data were processed using Thermo Scientific™ Proteome Discoverer™ 2.2 software.

Immunofluorescence and confocal imaging

Cells were fixed by 4% paraformaldehyde and incubated with specific antibody raised in rabbit followed by Alexa Fluro®568 conjugated anti-rabbit IgG secondary antibody (Thermo Fisher Scientific Inc., A10042), then stained with another mouse antibody followed by Alexa Fluro®674 conjugated anti-mouse IgG secondary antibodies (Thermo Fisher Scientific Inc., A31517). Conventional microscopy was performed with a Leica TCS SP8 confocal microscope. Cellular puncta formed by ATG13 or WIPI2 were quantified by ImageJ software (NIH, Bethesta, MD, US). Each data point was collected on ~ 100 cells from 4–5 separated views within the same samples. Cell number was counted by DAPI staining. Detailed information on chemicals and reagents were listed in Table 5.

Mitochondria fractionation

HeLa or HEK293T (2×10^7) cells were resuspended in 0.5 ml of mitochondrial extraction buffer (210 mM mannitol, 70 mM sucrose, 10 mM Tris-HCl pH 7.5, and 1 mM EDTA pH 7.5). Cell homogenate was obtained by disrupting cell membrane through a 27-gauge needle for 10 strokes. The degree of homogenization was monitored with a phase-contrast microscope. The homogenate was first centrifuged at 1500 × g for 5 min to remove nuclei and cell debris. The supernatant was transferred to a new tube and a second centrifugation was carried out at 10,000 × g for 15 min to pellet down mitochondria. The upper supernatant was saved as cytosolic fraction, and the mitochondria pellet was washed with mitochondrial extraction buffer and centrifuged again at 10,000 × g for 15 min. These crude mitochondria pellet was then lysed in the RIPA lysis buffer (25 mM Tris-HCl pH 7.5, 150 mM NaCl, 1% NP-40, 0.1% SDS and 0.5% sodium deoxycholate (Sigma-Aldrich CO. LLC, 30970) for western blot analysis. The entire process of mitochondria isolation was performed on ice or at 4°C. Protease inhibitors were included in all buffers. The cytosolic fractions were supplemented with ice-cold trichloroacetic acid (TCA) (Sigma-Aldrich CO. LLC, T6399), incubated on ice for 20 min, followed by top speed centrifugation at 4°C for 10 min. The pellet was then washed with pre-chilled acetone for 2 times. The protein pellet was then air dried for a few minutes before re-dissolved in SDS sample buffer. Both the mitochondrial fraction and cytosolic fraction were then subject to western blot analysis.

CHX chase assay

Cells were transfected with indicated plasmids. After that, cells were treated with 50 μg/ml CHX and were collected at each indicated time point for immunoblot analysis.

GFP-LC3-RFP-LC3ΔG autophagy reporter assay

Stable HeLa cell lines were generated using a GFP-LC3-RFP-LC3ΔG [82] plasmid by puromycin selection. Cell samples were then examined by Leica SP8 confocal microscope. Alternatively, cells were seeded in 96-well plates at 30,000 cells/well and grown overnight. After drug treatment or genetic manipulations, cells were fixed with 4% PFA in PBS for 10 min and washed with PBS. Measurement of GFP and RFP fluorescence was performed using a Synergy H1 plate reader (BioTek) with excitation/emission at 487/515 nm and 581/608 nm, respectively.

Stereotaxic injections

Mice were anesthetized with ketamine (200 mg/kg) and xylazine (10 mg/kg) and placed in a stereotaxic frame. Ophthalmic eye ointment was applied to prevent desiccation of the cornea during surgery. The area around the incision was trimmed and disinfected. PBS or mouse SNCA PFF (5 μg/side) or PFF with virus ~1×10^{10} GC was injected into the striatum (anteroposterior = +0.5 mm, mediolateral = ±1.8 mm, depth = −3.0 mm, relative to bregma). 5 μL volume was injected at a rate of 0.5 μL/min using a 5 μL Hamilton syringe. To limit reflux along the injection track, the needle was maintained in situ for 5 min, before being slowly retrieved. Each mouse was treated with baytril and meloxicam in the water bottle and monitored during recovery for one week.

Table 4. Antibodies.

Antibodies	Resource	Identifier
CHCHD2	Sigma-Aldrich Co. LLC	HPA027407
	Thermo Fisher Scientific Inc.	PA5-23564
	Proteintech Group, Inc	19424-1-AP
CHCHD10	Sigma-Aldrich Co. LLC	HPA003440
	Abcam	ab121196
	RayBiotech Inc	102-12935
	Proteintech Group, Inc	25671-1-AP
C1QBP/p32	Abcam	ab24733
	Proteintech Group, Inc	24474-1-AP
LAMP2A	Abcam	ab18528
HSPA8/HSC70 (13D3)	Thermo Fisher Scientific Inc.	MA3-014
LAMP1	Cell Signaling Technology	15665S
HSPD1/HSP60	Proteintech Group, Inc	66041-1-Ig
LONP1	Proteintech Group, Inc	15440–1-AP
CLPP	Santa Cruz Biotechnology	sc-134496
HTRA2	Santa Cruz Biotechnology	sc-15467
AFG3L2	Proteintech Group, Inc	14631–1-AP
YME1L1	Proteintech Group, Inc	11510–1-AP
SQSTM1/p62	Proteintech Group, Inc	66184-1-Ig
	Cell Signaling Technology	8025S
Ubiquitin/UB	Santa Cruz Biotechnology	sc-8017
PARK7/DJ-1	Santa Cruz Biotechnology	sc-55572
TOMM20	Santa Cruz Biotechnology	sc-17764
SNCA/α-Synuclein (Full length epitope)	BD (Becton, Dickinson and Company)	610787
SNCA/α-Synuclein (C-terminal epitope)	Abcam	ab6162
ATG5	Cell Signaling Technology	12994
ATG7	Cell Signaling Technology	8558
ULK1	Cell Signaling Technology	8054
ATG13	Cell Signaling Technology	13468T
RB1CC1	Cell Signaling Technology	12436
BECN1/Beclin 1	Cell Signaling Technology	3495
p-S30-BECN1/Beclin 1	Cell Signaling Technology	35955S
WIPI2	Cell Signaling Technology	ab105459
TFEB	Cell Signaling Technology	37785
MAP1LC3A/B	Cell Signaling Technology	12741
GABARAP	Santa Cruz Biotechnology	sc-377300
GABARAPL1	Proteintech Group, Inc	11010-1-AP
GABARAPL2	Proteintech Group, Inc	18724-1-AP
OPTN	Proteintech Group, Inc	10837-1-AP
ACTB	Sigma-Aldrich Co. LLC	A5441
GAPDH	Cell signaling Technology	2118
GST	Santa Cruz Biotechnology	sc-138
6×His	Thermo Fisher Scientific Inc.	MA1-21315
FLAG	Proteintech Group	80010-1-rr
	Sigma-Aldrich Co. LLC	F3165
HA	Proteintech Group	66006-2-Ig
MYC/c-Myc (9E10)	Santa Cruz Biotechnology	sc-40
GFP	Proteintech Group	66002-1-Ig
TH	Pel-Freeze	P40101-150
NR4A2/NURR1	Sigma-Aldrich CO. LLC	ABE1455
FOXA2	Santa Cruz Biotechnology	sc-101060
TUBB3	Millipore, Merck & Co., Inc	SAB4700544
PDH	Cell Signaling Technology	3205
TIMM50	Proteintech Group, Inc	22229-1-AP
p-Ser29-ATG14	Cell Signaling Technology	92340
ATG14	Cell Signaling Technology	96752

Cell or mice tissue extraction and western blotting

Mouse brain tissue was subdissected, snap-frozen and stored at -80°C until further use. In vitro, iPS cells and neurons were washed with ice-cold PBS prior to lysis. Cells or tissue was lysed on ice in 1× RIPA lysis buffer or sequentially in 1% Triton X-100 followed by 2% SDS lysis buffer supplemented with protease and phosphatase inhibitor cocktail (Sigma-Aldrich Co. LLC, 11836170001, 4906845001). Crude RIPA lysates were centrifuged at 15,000 × *g* for 10 min at 4°C to remove cellular debris. Triton X-100 lysates were centrifuged at approximately 15,000 × *g* for 10 min at 4°C. The pellet was resuspended and sonicated in 2% SDS lysis buffer. Clarified lysates were quantified with a Pierce BCA protein assay. Cell lysates were mixed with Laemmli buffer and equal amounts of protein were subjected to SDS-PAGE. Cell or tissue lysates were subjected to electrophoresis on 6-15% SDS-PAGE gels and separated proteins were transferred electrophoretically to PVDF or nitrocellulose membranes, which were blocked with 5% nonfat milk or BSA, and then incubated with primary antibodies followed by HRP-conjugated secondary antibodies. Signals were detected by Fuji Xejo Imaging system. Protein bands on blots were quantified by ImageJ software (NIH, Bethesta, MD, US).

Real time-quantitative PCR

Total RNA was extracted by RNeasy Kit (Qiagen, 74104), was then reversely transcribed using iScript™ Select cDNA Synthesis Kit (Bio-Rad Laboratories, Inc, 1708896). Real-Time PCR was performed with SsoFast™ EvaGreen®

Table 5. Chemicals and reagents.

Name	Resource	Identifier
CDDO	Cayman Chemical	81035-1
FCCP	Abcam	ab120081
CHX	Sigma-Aldrich CO. LLC	C7698
MG132	Sigma-Aldrich CO, LLC	C2211
AR-7	Sigma-Aldrich CO. LLC	SML0921
leupeptin	Tocris Bioscience	1167/25
rapamycin	LC laboratories	R-5000
NH_4Cl	Sigma-Aldrich CO. LLC	A9434
chloroquine	Sigma-Aldrich CO. LLC	C6628
puromycin	Thermo Fisher Scientific Inc.	A1113803
wortmannin	MedChemExpress LLC	HY-10197
torin 1	MedChemExpress LLC	HY-13003
bafilomycin A_1	MedChemExpress LLC	HY-100558
SNAP-Cell® TMR-Star	New England Biolabs, Inc.	S9105S
SNAP-Cell® 505-Star	New England Biolabs, Inc	S9103S
MitoTracker™ Deep Red	Thermo Fisher Scientific Inc.	M22426
ProteoStat® Aggresome Detection Kit	Enzo Life Sciences	ENZ-51035-K100
GST beads	Pierce™, Thermo Scientific	16100
Ni-NTA beads	QIAGEN, N.V.	1018244
BL21(DE3)	New England Biolabs, Inc	C2527I
SHuffle® T7	New England Biolabs, Inc	C3029J
AAV-CBh-hCHCHD2 (WT)	Vector Biolabs	N/A
SNCA/Alpha-Synuclein Preformed Fibril (human)	rPeptide	ASF-1001–01
Active Mouse Recombinant SNCA/Alpha Synuclein Pre-Formed Fibrils (Type 1)	StressMarq Biosciences	SPR-324
MAPT/Tau-441 Preformed Fibrils	rPeptide	TF-1001–2
Pierce BCA protein assay	Thermo Fisher Scientific Inc.	23225

Supermix (Bio-Rad Laboratories, Inc, 1725211) on Applied Biosystems 7500 Fast RT-qPCR system using gene-specific primers [120]. Ct values for genes of interest were collected during the log phase of the cycle. Quantification of targeted mRNA was normalized against *ACTB* mRNA using ΔΔCt method.

Statistics and reproducibility

All experiments were carried out with at least 3 independent biological replicates. The statistics methods were indicated in respective figure legends.

Acknowledgements

We thank Prof. Ling Shuo-Chien (National University of Singapore) for FUS plasmids. We thank Prof Lim Kah Leong (Nanyang Technological University, Singapore) for helpful discussion. We thank Ms Keshmarathy D/O Sacadevan from SingHealth Advanced Bioimaging Core for supports on confocal microscopy.

Author contributions

CRediT: **Wei Zhou:** Conceptualization, Data curation, Formal analysis, Investigation, Methodology, Project administration, Resources, Software, Supervision, Validation, Visualization, Writing – original draft, Writing – review & editing; **Maggie Menglan Zhang:** Methodology, Resources; **Willcyn Tang:** Investigation, Methodology, Resources, Software; **Brijesh Kumar Singh:** Investigation, Methodology, Resources; **Zhiwei Zhang:** Investigation, Methodology, Resources; **Lei Zhou:** Investigation, Methodology; **Jaron Kim Wee Goh:** Formal analysis, Investigation; **Faith Rui En Tan:** Formal analysis, Investigation, Methodology; **Jingxiu Huang:** Methodology; **Qiaoyang Sun:** Formal analysis; **Bin Xiao:** Resources; **Gupta Priyanka:** Investigation, Methodology; **Alfred Xuyang Sun:** Investigation, Methodology, Resources; **Li Zeng:** Resources, Writing – review & editing; **Han-Ming Shen:** Resources, Supervision, Writing – review & editing; **Eng King Tan:** Funding acquisition, Resources, Supervision, Writing – review & editing.

Disclosure statement

No potential conflict of interest was reported by the author(s).

Funding

This research is supported by Singapore Ministry of Health's National Medical Research Council under its Open Fund Large Collaborative Grant [MOH-OFLCG24may-0004] and Singapore Translational Research (STaR) Investigator Award [NMRC/STaR/0030/2018] to Prof Tan EK. LZ is supported by InnoHK initiative of the Innovation and Technology Commission of the Hong Kong Special Administrative Region Government.

Data availability statement

Supplemental data for this article can be accessed on the publisher's website. Any additional materials are available from the corresponding author upon reasonable request.

ORCID

Wei Zhou http://orcid.org/0000-0002-0872-6223
Willcyn Tang http://orcid.org/0000-0002-3739-1784
Brijesh Kumar Singh http://orcid.org/0000-0003-4615-3988
Qiaoyang Sun http://orcid.org/0000-0002-7842-7034
Alfred Xuyang Sun http://orcid.org/0000-0002-7893-2006
Li Zeng http://orcid.org/0000-0003-3242-2286
Han-Ming Shen http://orcid.org/0000-0001-7369-5227
Eng King Tan http://orcid.org/0000-0003-2977-9743

References

[1] Funayama M, Ohe K, Amo T, et al. CHCHD2 mutations in autosomal dominant late-onset Parkinson's disease: a genome-wide linkage and sequencing study. Lancet Neurol. 2015;14 (3):274–282. doi: 10.1016/S1474-4422(14)70266-2

[2] Liu Z, Guo J, Li K, et al. Mutation analysis of CHCHD2 gene in Chinese familial Parkinson's disease. Neurobiol Aging. 2015;36 (11): e31177–e31178. doi: 10.1016/j.neurobiolaging.2015.08.010

[3] Koschmidder E, Weissbach A, Brüggemann N, et al. A nonsense mutation in CHCHD2 in a patient with Parkinson disease. Neurology. 2016;86(6):577–579. doi: 10.1212/WNL.0000000000002361

[4] Shi CH, Mao C-Y, Zhang S-Y, et al. CHCHD2 gene mutations in familial and sporadic Parkinson's disease. Neurobiol Aging. 2016;38: e2179–e21713. doi: 10.1016/j.neurobiolaging.2015.10.040

[5] Zhang M, Xi Z, Fang S, et al. Mutation analysis of CHCHD2 in Canadian patients with familial Parkinson's disease. Neurobiol Aging. 2016;38: e2177–e2178. doi: 10.1016/j.neurobiolaging.2015.10.038

[6] Rubino E, Brusa L, Zhang M, et al. Genetic analysis of CHCHD2 and CHCHD10 in Italian patients with Parkinson's disease. Neurobiol Aging. 2017;53: e1937–e1938. doi: 10.1016/j.neurobiolaging.2016.12.027

[7] Che XQ, Zhao Q-H, Huang Y, et al. Mutation screening of the CHCHD2 gene for Alzheimer's disease and frontotemporal dementia in Chinese mainland population. J Alzheimers Dis. 2018;61(4):1283–1288. doi: 10.3233/JAD-170692

[8] Liu X, Jiao B, Zhang W, et al. Identification of CHCHD2 mutations in patients with Alzheimer's disease, amyotrophic lateral sclerosis and frontotemporal dementia in China. Mol Med Rep. 2018;18(1):461–466. doi: 10.3892/mmr.2018.8962

[9] Gao C, Chen Y-M, Sun Q, et al. Mutation analysis of CHCHD2 gene in Chinese Han familial essential tremor patients and familial Parkinson's disease patients. Neurobiol Aging. 2017;49: e2189–e21811. doi: 10.1016/j.neurobiolaging.2016.10.001

[10] Yang X, An R, Zhao Q, et al. Mutational analysis of CHCHD2 in Chinese patients with multiple system atrophy and amyotrophic lateral sclerosis. J Neurol Sci. 2016;368:389–391. doi: 10.1016/j.jns.2016.07.063

[11] Ikeda A, Meng H, Taniguchi D, et al. CHCHD2 P14L, found in amyotrophic lateral sclerosis, exhibits cytoplasmic mislocalization and alters Ca(2+) homeostasis. PNAS Nexus. 2024;3(8):pgae319. doi: 10.1093/pnasnexus/pgae319

[12] Straub IR, Janer A, Weraarpachai W, et al. Loss of CHCHD10-CHCHD2 complexes required for respiration underlies the pathogenicity of a CHCHD10 mutation in ALS. Hum Mol Genet. 2018;27(1):178–189. doi: 10.1093/hmg/ddx393

[13] Huang X, Wu BP, Nguyen D, et al. CHCHD2 accumulates in distressed mitochondria and facilitates oligomerization of CHCHD10. Hum Mol Genet. 2019;28(2):349. doi: 10.1093/hmg/ddy340

[14] Zhou W, Ma D, Sun AX, et al. PD-linked CHCHD2 mutations impair CHCHD10 and MICOS complex leading to mitochondria dysfunction. Hum Mol Genet. 2019;28(7):1100–1116. doi: 10.1093/hmg/ddy413

[15] Chaussenot A, Le Ber I, Ait-El-Mkadem S, et al. Screening of CHCHD10 in a French cohort confirms the involvement of this gene in frontotemporal dementia with amyotrophic lateral sclerosis patients. Neurobiol Aging. 2014;35(12): e28841–e28844. doi: 10.1016/j.neurobiolaging.2014.07.022

[16] Dols-Icardo O, Nebot I, Gorostidi A, et al. Analysis of the CHCHD10 gene in patients with frontotemporal dementia and amyotrophic lateral sclerosis from Spain. Brain. 2015;138(12): e400. doi: 10.1093/brain/awv175

[17] Jiao B, Xiao T, Hou L, et al. High prevalence of CHCHD10 mutation in patients with frontotemporal dementia from China. Brain. 2016;139(4):e21. doi: 10.1093/brain/awv367

[18] Teyssou E, Chartier L, Albert M, et al. Genetic analysis of CHCHD10 in French familial amyotrophic lateral sclerosis patients. Neurobiol Aging. 2016;42:218 e1–3. doi: 10.1016/j.neurobiolaging.2016.03.022

[19] Johnson JO, Glynn SM, Gibbs JR, et al. Mutations in the CHCHD10 gene are a common cause of familial amyotrophic lateral sclerosis. Brain. 2014;137(12):e311. doi: 10.1093/brain/awu265

[20] Ajroud-Driss S, Fecto F, Ajroud K, et al. Mutation in the novel nuclear-encoded mitochondrial protein CHCHD10 in a family with autosomal dominant mitochondrial myopathy. Neurogenetics. 2015;16(1):1–9. doi: 10.1007/s10048-014-0421-1

[21] Auranen M, Ylikallio E, Shcherbii M, et al. CHCHD10 variant p.(Gly66Val) causes axonal charcot-marie-tooth disease. Neurol Genet. 2015;1(1):e1. doi: 10.1212/NXG.0000000000000003

[22] Pasanen P, Myllykangas L, Pöyhönen M, et al. Intrafamilial clinical variability in individuals carrying the CHCHD10 mutation Gly66Val. Acta Neurol Scand. 2016;133(5):361–366. doi: 10.1111/ane.12470

[23] Woo J-A-A, Liu T, Trotter C, et al. Loss of function CHCHD10 mutations in cytoplasmic TDP-43 accumulation and synaptic integrity. Nat Commun. 2017;8(1):15558. doi: 10.1038/ncomms15558

[24] Meng H, Yamashita C, Shiba-Fukushima K, et al. Loss of Parkinson's disease-associated protein CHCHD2 affects mitochondrial crista structure and destabilizes cytochrome c. Nat Commun. 2017;8(1):15500. doi: 10.1038/ncomms15500

[25] Tio M, Wen R, Lim YL, et al. Varied pathological and therapeutic response effects associated with CHCHD2 mutant and risk variants. Hum Mutat. 2017;38(8):978–987. doi: 10.1002/humu.23234

[26] Liu W, Duan X, Xu L, et al. Chchd2 regulates mitochondrial morphology by modulating the levels of Opa1. Cell Death Differ. 2020;27(6):2014–2029. doi: 10.1038/s41418-019-0482-7

[27] Baek M, Choe Y-J, Bannwarth S, et al. TDP-43 and PINK1 mediate CHCHD10(S59L) mutation-induced defects in Drosophila and in vitro. Nat Commun. 2021;12(1):1924. doi: 10.1038/s41467-021-22145-9

[28] Petel Legare V, Rampal CJ, Gurberg TJN, et al. Loss of mitochondrial Chchd10 or Chchd2 in zebrafish leads to an ALS-like phenotype and complex I deficiency independent of the mitochondrial integrated stress response. Dev Neurobiol. 2023;83(1–2):54–69. doi: 10.1002/dneu.22909

[29] Sato S, Noda S, Torii S, et al. Homeostatic p62 levels and inclusion body formation in CHCHD2 knockout mice. Hum Mol Genet. 2021;30(6):443–453. doi: 10.1093/hmg/ddab057

[30] Fan L, Zhang S, Li X, et al. CHCHD2 p.Thr61Ile knock-in mice exhibit motor defects and neuropathological features of Parkinson's disease. Brain Pathol. 2023;33(3):e13124. doi: 10.1111/bpa.13124

[31] Kee TR, Wehinger JL, Gonzalez PE, et al. Pathological characterization of a novel mouse model expressing the PD-linked CHCHD2-T61I mutation. Hum Mol Genet. 2022;31(23):3987–4005. doi: 10.1093/hmg/ddac083

[32] Torii S, Arakawa S, Sato S, et al. Involvement of casein kinase 1 epsilon/delta (Csnk1e/d) in the pathogenesis of familial Parkinson's disease caused by CHCHD2. EMBO Mol Med. 2023;15(9):e17451. doi: 10.15252/emmm.202317451

[33] Ryan EB, Yan J, Miller N, et al. Early death of ALS-linked CHCHD10-R15L transgenic mice with central nervous system, skeletal muscle, and cardiac pathology. iScience. 2021;24(2):102061. doi: 10.1016/j.isci.2021.102061

[34] Liu T, Woo J-A-A, Bukhari MZ, et al. Modulation of synaptic plasticity, motor unit physiology, and TDP-43 pathology by CHCHD10. Acta Neuropathol Commun. 2022;10(1):95. doi: 10.1186/s40478-022-01386-9

[35] Anderson CJ, Bredvik K, Burstein SR, et al. ALS/FTD mutant CHCHD10 mice reveal a tissue-specific toxic gain-of-function and mitochondrial stress response. Acta Neuropathol. 2019;138(1):103–121. doi: 10.1007/s00401-019-01989-y

[36] Genin EC, Madji Hounoum B, Bannwarth S, et al. Mitochondrial defect in muscle precedes neuromuscular junction degeneration and motor neuron death in CHCHD10(S59L/+) mouse. Acta Neuropathol. 2019;138(1):123–145. doi: 10.1007/s00401-019-01988-z

[37] Liu YT, Huang X, Nguyen D, et al. Loss of CHCHD2 and CHCHD10 activates OMA1 peptidase to disrupt mitochondrial cristae phenocopying patient mutations. Hum Mol Genet. 2020;29(9):1547–1567. doi: 10.1093/hmg/ddaa077

[38] Shammas MK, Huang X, Wu BP, et al. OMA1 mediates local and global stress responses against protein misfolding in CHCHD10 mitochondrial myopathy. J Clin Invest. 2022;132(14). doi: 10.1172/JCI157504

[39] Bannwarth S, Ait-El-Mkadem S, Chaussenot A, et al. A mitochondrial origin for frontotemporal dementia and amyotrophic lateral sclerosis through CHCHD10 involvement. Brain. 2014;137(8):2329–2345. doi: 10.1093/brain/awu138

[40] Genin EC, Plutino M, Bannwarth S, et al. CHCHD10 mutations promote loss of mitochondrial cristae junctions with impaired mitochondrial genome maintenance and inhibition of apoptosis. EMBO Mol Med. 2016;8(1):58–72. doi: 10.15252/emmm.201505496

[41] Burstein SR, Valsecchi F, Kawamata H, et al. In vitro and in vivo studies of the ALS-FTLD protein CHCHD10 reveal novel mitochondrial topology and protein interactions. Hum Mol Genet. 2018;27(1):160–177. doi: 10.1093/hmg/ddx397

[42] Liu Y, Clegg HV, Leslie PL, et al. CHCHD2 inhibits apoptosis by interacting with bcl-x L to regulate Bax activation. Cell Death Differ. 2015;22(6):1035–1046. doi: 10.1038/cdd.2014.194

[43] Gao G, Shi Y, Deng H-X, et al. Dysregulation of mitochondrial alpha-ketoglutarate dehydrogenase leads to elevated lipid peroxidation in CHCHD2-linked Parkinson's disease models. Nat Commun. 2025;16(1):1982. doi: 10.1038/s41467-025-57142-9

[44] Nguyen MK, McAvoy K, Liao S-C, et al. Mouse midbrain dopaminergic neurons survive loss of the PD-associated mitochondrial protein CHCHD2. Hum Mol Genet. 2022;31(9):1500–1518. doi: 10.1093/hmg/ddab329

[45] Harjuhaahto S, Rasila TS, Molchanova SM, et al. ALS and Parkinson's disease genes CHCHD10 and CHCHD2 modify synaptic transcriptomes in human iPSC-derived motor neurons. Neurobiol Dis. 2020;141:104940. doi: 10.1016/j.nbd.2020.104940

[46] Lv G, Sayles NM, Huang Y, et al. Amyloid fibril structures link CHCHD10 and CHCHD2 to neurodegeneration. Nat Commun. 2025;16(1):7121. doi: 10.1038/s41467-025-62149-3

[47] Ikeda A, Nishioka K, Meng H, et al. Mutations in CHCHD2 cause alpha-synuclein aggregation. Hum Mol Genet. 2019;28(23):3895–3911. doi: 10.1093/hmg/ddz241

[48] Keith JL, Swinkin E, Gao A, et al. Neuropathologic description of CHCHD10 mutated amyotrophic lateral sclerosis. Neurol Genet. 2020;6(1):e394. doi: 10.1212/NXG.0000000000000394

[49] Sayles NM, Southwell N, McAvoy K, et al. Mutant CHCHD10 causes an extensive metabolic rewiring that precedes OXPHOS dysfunction in a murine model of mitochondrial cardiomyopathy. Cell Rep. 2022;38(10):110475. doi: 10.1016/j.celrep.2022.110475

[50] Wei Y, Vellanki RN, Coyaud É, et al. CHCHD2 is coamplified with EGFR in NSCLC and regulates mitochondrial function and Cell migration. Mol Cancer Res. 2015;13(7):1119–1129. doi: 10.1158/1541-7786.MCR-14-0165-T

[51] Chen R, Xiao M, Gao H, et al. Identification of a novel mitochondrial interacting protein of C1QBP using subcellular fractionation coupled with CoIP-MS. Anal Bioanal Chem. 2016;408(6):1557–1564. doi: 10.1007/s00216-015-9228-7

[52] Ren YL, Jiang Z, Wang J-Y, et al. Loss of CHCHD2 stability coordinates with C1QBP/CHCHD2/CHCHD10 complex impairment to mediate PD-Linked mitochondrial dysfunction. Mol Neurobiol. 2024;61(10):7968–7988. doi: 10.1007/s12035-024-04090-y

[53] Feichtinger RG, Oláhová M, Kishita Y, et al. Biallelic C1QBP mutations cause severe neonatal-, childhood-, or later-onset cardiomyopathy associated with combined respiratory-chain deficiencies. Am J Hum Genet. 2017;101(4):525–538. doi: 10.1016/j.ajhg.2017.08.015

[54] Webster G, Reynolds M, Arva NC, et al. Mitochondrial cardiomyopathy and ventricular arrhythmias associated with biallelic variants in C1QBP. Am J Med Genet A. 2021;185(8):2496–2501. doi: 10.1002/ajmg.a.62262

[55] Alstrup M, Vogel I, Sandager P, et al. A novel homozygous variant in C1QBP causes severe IUGR, edema, and cardiomyopathy in two fetuses. JIMD Rep. 2021;59(1):20–25. doi: 10.1002/jmd2.12209

[56] Wang J, Li H, Sun M, et al. Early onset of combined oxidative phosphorylation deficiency in two Chinese Brothers caused by a homozygous (Leu275Phe) mutation in the C1QBP gene. Front Pediatr. 2020;8:583047. doi: 10.3389/fped.2020.583047

[57] Yagi M, Uchiumi T, Sagata N, et al. Neural-specific deletion of mitochondrial p32/C1qbp leads to leukoencephalopathy due to undifferentiated oligodendrocyte and axon degeneration. Sci Rep. 2017;7(1):15131. doi: 10.1038/s41598-017-15414-5

[58] Saito T, Uchiumi T, Yagi M, et al. Cardiomyocyte-specific loss of mitochondrial p32/C1qbp causes cardiomyopathy and activates stress responses. Cardiovasc Res. 2017;113(10):1173–1185. doi: 10.1093/cvr/cvx095

[59] Yagi M, Toshima T, Amamoto R, et al. Mitochondrial translation deficiency impairs NAD(+) -mediated lysosomal acidification. Embo J. 2021;40(8):e105268. doi: 10.15252/embj.2020105268

[60] Ruan Y, Hu J, Che Y, et al. CHCHD2 and CHCHD10 regulate mitochondrial dynamics and integrated stress response. Cell Death Dis. 2022;13(2):156. doi: 10.1038/s41419-022-04602-5

[61] Li C, Wang X, Li X, et al. Proteasome inhibition activates autophagy-lysosome pathway associated with TFEB dephosphorylation and nuclear translocation. Front Cell Dev Biol. 2019;7:170. doi: 10.3389/fcell.2019.00170

[62] Lehmer C, Schludi MH, Ransom L, et al. A novel CHCHD10 mutation implicates a Mia40-dependent mitochondrial import deficit in ALS. EMBO Mol Med. 2018;10(6). doi: 10.15252/emmm.201708558

[63] Ikeda A, Imai Y, Hattori N. Neurodegeneration-associated mitochondrial proteins, CHCHD2 and CHCHD10-what distinguishes the two? Front Cell Dev Biol. 2022;10:996061. doi: 10.1007/978-1-4939-8873-0_47

[64] Stephan T, Roesch A, Riedel D, et al. Live-cell STED nanoscopy of mitochondrial cristae. Sci Rep. 2019;9(1):12419. doi: 10.1038/s41598-019-48838-2

[65] Xu CY, Kang W-Y, Chen Y-M, et al. DJ-1 inhibits alpha-synuclein aggregation by regulating chaperone-mediated autophagy. Front Aging Neurosci. 2017;9:308. doi: 10.3389/fnagi.2017.00308

[66] Seki T, Yoshino K-I, Tanaka S, et al. Establishment of a novel fluorescence-based method to evaluate chaperone-mediated autophagy in a single neuron. PLOS ONE. 2012;7(2):e31232. doi: 10.1371/journal.pone.0031232

[67] Kaushik S, Cuervo AM. The coming of age of chaperone-mediated autophagy. Nat Rev Mol Cell Biol. 2018;19(6):365–381. doi: 10.1038/s41580-018-0001-6

[68] Juste YR, Cuervo AM. Analysis of chaperone-mediated autophagy. Methods Mol Biol. 2019;1880:703–727. doi: 10.1007/978-1-4939-8873-0_47

[69] Jiang J, Zhang Y, Krainer AR, et al. Crystal structure of human p32, a doughnut-shaped acidic mitochondrial matrix protein. Proc Natl Acad Sci USA. 1999;96(7):3572–3577. doi: 10.1073/pnas.96.7.3572

[70] Johansen T, Lamark T. Selective autophagy: ATG8 family proteins, LIR motifs and cargo receptors. J Mol Biol. 2020;432(1):80–103. doi: 10.1016/j.jmb.2019.07.016

[71] Imai Y, Meng H, Shiba-Fukushima K, et al. Twin CHCH proteins, CHCHD2, and CHCHD10: key molecules of Parkinson's disease, amyotrophic lateral sclerosis, and frontotemporal dementia. Int J Mol Sci. 2019;20(4):908. doi: 10.3390/ijms20040908

[72] Zhou W, Ma D, Tan EK. Mitochondrial CHCHD2 and CHCHD10: roles in neurological diseases and therapeutic implications. Neuroscientist. 2020;26(2):170–184. doi: 10.1177/1073858419871214

[73] Polyansky AA, Chugunov AO, Volynsky PE, et al. PREDDIMER: a web server for prediction of transmembrane helical dimers. Bioinformatics. 2014;30(6):889–890. doi: 10.1093/bioinformatics/btt645

[74] Rogov VV, Nezis IP, Tsapras P, et al. Atg8 family proteins, LIR/AIM motifs and other interaction modes. Autophagy Rep. 2023;2(1). doi: 10.1080/27694127.2023.2188523

[75] Shpilka T, Weidberg H, Pietrokovski S, et al. Atg8: an autophagy-related ubiquitin-like protein family. Genome Biol. 2011;12(7):226. doi: 10.1186/gb-2011-12-7-226

[76] Honda S, Arakawa S, Yamaguchi H, et al. Association between Atg5-independent alternative autophagy and neurodegenerative diseases. J Mol Biol. 2020;432(8):2622–2632. doi: 10.1016/j.jmb.2020.01.016

[77] Cornelissen T, Spinazzi M, Martin S, et al. CHCHD2 harboring Parkinson's disease-linked T61I mutation precipitates inside mitochondria and induces precipitation of wild-type CHCHD2. Hum Mol Genet. 2020;29(7):1096–1106. doi: 10.1093/hmg/ddaa028

[78] Morishita H, Mizushima N. Diverse cellular roles of autophagy. Annu Rev Cell Dev Biol. 2019;35(1):453–475. doi: 10.1146/annurev-cellbio-100818-125300

[79] Hara T, Takamura A, Kishi C, et al. FIP200, a ULK-interacting protein, is required for autophagosome formation in mammalian cells. J Cell Biol. 2008;181(3):497–510. doi: 10.1083/jcb.200712064

[80] Grunwald DS, Otto NM, Park J-M, et al. Gabaraps and LC3s have opposite roles in regulating ULK1 for autophagy induction. Autophagy. 2020;16(4):600–614. doi: 10.1080/15548627.2019.1632620

[81] Dooley HC, Razi M, Polson HJ, et al. WIPI2 links LC3 conjugation with PI3P, autophagosome formation, and pathogen clearance by recruiting Atg12-5-16L1. Mol Cell. 2014;55(2):238–252. doi: 10.1016/j.molcel.2014.05.021

[82] Kaizuka T, Morishita H, Hama Y, et al. An autophagic flux probe that releases an internal control. Mol Cell. 2016;64(4):835–849. doi: 10.1016/j.molcel.2016.09.037

[83] Sarraf SA, Shah HV, Kanfer G, et al. Loss of TAX1BP1-directed autophagy results in protein aggregate accumulation in the brain. Mol Cell. 2020;80(5):779–795 e10. doi: 10.1016/j.molcel.2020.10.041

[84] Wetzel L, Blanchard S, Rama S, et al. TECPR1 promotes aggrephagy by direct recruitment of LC3C autophagosomes to lysosomes. Nat Commun. 2020;11(1):2993. doi: 10.1038/s41467-020-16689-5

[85] Volpicelli-Daley LA, Luk KC, Lee VM. Addition of exogenous alpha-synuclein preformed fibrils to primary neuronal cultures to seed recruitment of endogenous alpha-synuclein to Lewy body and Lewy neurite-like aggregates. Nat Protoc. 2014;9(9):2135–2146. doi: 10.1038/nprot.2014.143

[86] Daher JP, Ying M, Banerjee R, et al. Conditional transgenic mice expressing C-terminally truncated human alpha-synuclein (alphaSyn119) exhibit reduced striatal dopamine without loss of nigrostriatal pathway dopaminergic neurons. Mol Neurodegener. 2009;4(1):34. doi: 10.1186/1750-1326-4-34

[87] Ulusoy A, Febbraro F, Jensen PH, et al. Co-expression of C-terminal truncated alpha-synuclein enhances full-length alpha-synuclein-induced pathology. Eur J Neurosci. 2010;32(3):409–422. doi: 10.1111/j.1460-9568.2010.07284.x

[88] Volpicelli-Daley LA, Luk K, Patel T, et al. Exogenous alpha-synuclein fibrils induce Lewy body pathology leading to synaptic dysfunction and neuron death. Neuron. 2011;72(1):57–71. doi: 10.1016/j.neuron.2011.08.033

[89] Zhang C, Pei Y, Zhang Z, et al. C-terminal truncation modulates alpha-synuclein's cytotoxicity and aggregation by promoting the interactions with membrane and chaperone. Commun Biol. 2022;5(1):798. doi: 10.1038/s42003-022-03768-0

[90] Quintin S, Lloyd GM, Paterno G, et al. Cellular processing of alpha-synuclein fibrils results in distinct physiological C-terminal truncations with a major cleavage site at residue glu 114. J Biol Chem. 2023;299(7):104912. doi: 10.1016/j.jbc.2023.104912

[91] Fogal V, Richardson AD, Karmali PP, et al. Mitochondrial p32 protein is a critical regulator of tumor metabolism via maintenance of oxidative phosphorylation. Mol Cell Biol. 2010;30(6):1303–1318. doi: 10.1128/MCB.01101-09

[92] Yin Z, Pascual C, Klionsky DJ. Autophagy: machinery and regulation. Microb Cell. 2016;3(12):588–596. doi: 10.15698/mic2016.12.546

[93] Li J, Cai Z, Vaites LP, et al. Proteome-wide mapping of short-lived proteins in human cells. Mol Cell. 2021;81(22):4722–4735 e5. doi: 10.1016/j.molcel.2021.09.015

[94] Aras S, Pak O, Sommer N, et al. Oxygen-dependent expression of cytochrome c oxidase subunit 4–2 gene expression is mediated by transcription factors RBPJ, CXXC5 and CHCHD2. Nucleic Acids Res. 2013;41(4):2255–2266. doi: 10.1093/nar/gks1454

[95] Li Y, Xiu W, Xu J, et al. Increased CHCHD2 expression promotes liver fibrosis in nonalcoholic steatohepatitis via Notch/osteopontin signaling. JCI Insight. 2022;7(23). doi: 10.1172/jci.insight.162402

[96] Gu X, Nardone C, Kamitaki N, et al. The midnolin-proteasome pathway catches proteins for ubiquitination-independent degradation. Science. 2023;381(6660):eadh5021. doi: 10.1126/science.adh5021

[97] Obara Y, Imai T, Sato H, et al. Midnolin is a novel regulator of parkin expression and is associated with Parkinson's disease. Sci Rep. 2017;7(1):5885. doi: 10.1038/s41598-017-05456-0

[98] Sato H, Ishii K, Obara Y. Structural variants of midnolin, a Genetic risk factor for Parkinson's disease, in a Yamagata Cohort. Biol Pharm Bull. 2023;46(3):379–381. doi: 10.1248/bpb.b22-00776

[99] Aras S, Bai M, Lee I, et al. MNRR1 (formerly CHCHD2) is a bi-organellar regulator of mitochondrial metabolism. Mitochondrion. 2015;20:43–51. doi: 10.1016/j.mito.2014.10.003

[100] Aras S, Purandare N, Gladyck S, et al. Mitochondrial nuclear retrograde regulator 1 (MNRR1) rescues the cellular phenotype of MELAS by inducing homeostatic mechanisms. Proc Natl Acad Sci USA. 2020;117(50):32056–32065. doi: 10.1073/pnas.2005877117

[101] El-Brolosy MA, Stainier DYR. Genetic compensation: a phenomenon in search of mechanisms. PLOS Genet. 2017;13(7):e1006780. doi: 10.1371/journal.pgen.1006780

[102] Ma X, Lu C, Chen Y, et al. CCT2 is an aggrephagy receptor for clearance of solid protein aggregates. Cell. 2022;185(8):1325–1345 e22. doi: 10.1016/j.cell.2022.03.005

[103] Lim J, Yue Z. Neuronal aggregates: formation, clearance, and spreading. Dev Cell. 2015;32(4):491–501. doi: 10.1016/j.devcel.2015.02.002

[104] Yoon MJ, Choi B, Kim EJ, et al. UXT chaperone prevents proteotoxicity by acting as an autophagy adaptor for p62-dependent aggrephagy. Nat Commun. 2021;12(1):1955. doi: 10.1038/s41467-021-22252-7

[105] Lu K, Psakhye I, Jentsch S. Autophagic clearance of polyQ proteins mediated by ubiquitin-Atg8 adaptors of the conserved CUET protein family. Cell. 2014;158(3):549–563. doi: 10.1016/j.cell.2014.05.048

[106] Filimonenko M, Isakson P, Finley KD, et al. The selective macroautophagic degradation of aggregated proteins requires the PI3P-binding protein Alfy. Mol Cell. 2010;38(2):265–279. doi: 10.1016/j.molcel.2010.04.007

[107] Chen Y, Liu Z, Zhang Y, et al. Two distinct regulatory pathways govern Cct2-Atg8 binding in the process of solid aggrephagy. EMBO Rep. 2024;25(11):4749–4776. doi: 10.1038/s44319-024-00275-7

[108] Zhao YG, Zhang H. Phase separation in membrane biology: the interplay between membrane-bound organelles and membraneless condensates. Dev Cell. 2020;55(1):30–44. doi: 10.1016/j.devcel.2020.06.033

[109] Alberti S, Hyman AA. Biomolecular condensates at the nexus of cellular stress, protein aggregation disease and ageing. Nat Rev Mol Cell Biol. 2021;22(3):196–213. doi: 10.1038/s41580-020-00326-6

[110] Leitao ADG, Rudolffi-Soto P, Chappard A, et al. Selectivity of Lewy body protein interactions along the aggregation pathway of alpha-synuclein. Commun Biol. 2021;4(1):1124. doi: 10.1038/s42003-021-02624-x

[111] Jacquet M, Guittaut M, Fraichard A, et al. The functions of Atg8-family proteins in autophagy and cancer: linked or unrelated? Autophagy. 2021;17(3):599–611. doi: 10.1080/15548627.2020.1749367

[112] Wesch N, Kirkin V, Rogov VV. Atg8-family proteins-structural features and molecular interactions in autophagy and beyond. Cells. 2020;9(9):2008. doi: 10.3390/cells9092008

[113] Wang J, Huang CL, Zhang Y. Complement C1q binding protein (C1QBP): physiological functions, mutation-associated mitochondrial cardiomyopathy and Current disease models. Front Cardiovasc Med. 2022;9:843853. doi: 10.3389/fcvm.2022.843853

[114] Jiao H, Su G-Q, Dong W, et al. Chaperone-like protein p32 regulates ULK1 stability and autophagy. Cell Death Differ. 2015;22(11):1812–1823. doi: 10.1038/cdd.2015.34

[115] Wu W, Tian W, Hu Z, et al. ULK1 translocates to mitochondria and phosphorylates FUNDC1 to regulate mitophagy. EMBO Rep. 2014;15(5):566–575. doi: 10.1002/embr.201438501

[116] Liu X, Wang Q, Yang Y, et al. Reduced erythrocytic CHCHD2 mRNA is associated with brain pathology of Parkinson's disease. Acta Neuropathol Commun. 2021;9(1):37. doi: 10.1186/s40478-021-01133-6

[117] McCann EP, Fifita JA, Grima N, et al. Genetic and immunopathological analysis of CHCHD10 in Australian amyotrophic lateral sclerosis and frontotemporal dementia and transgenic TDP-43 mice. J Neurol Neurosurg Psychiatry. 2020;91(2):162–171. doi: 10.1136/jnnp-2019-321790

[118] Jo J, Xiao Y, Sun A, et al. Midbrain-like organoids from human pluripotent stem cells contain functional dopaminergic and neuromelanin-producing neurons. Cell STEM Cell. 2016;19(2):248–257. doi: 10.1016/j.stem.2016.07.005

[119] Sun S, Ling S-C, Qiu J, et al. ALS-causative mutations in FUS/TLS confer gain and loss of function by altered association with SMN and U1-snRNP. Nat Commun. 2015;6(1):6171. doi: 10.1038/ncomms7171

[120] Bordi M, De Cegli R, Testa B, et al. A gene toolbox for monitoring autophagy transcription. Cell Death Dis. 2021;12(11):1044. doi: 10.1038/s41419-021-04121-9